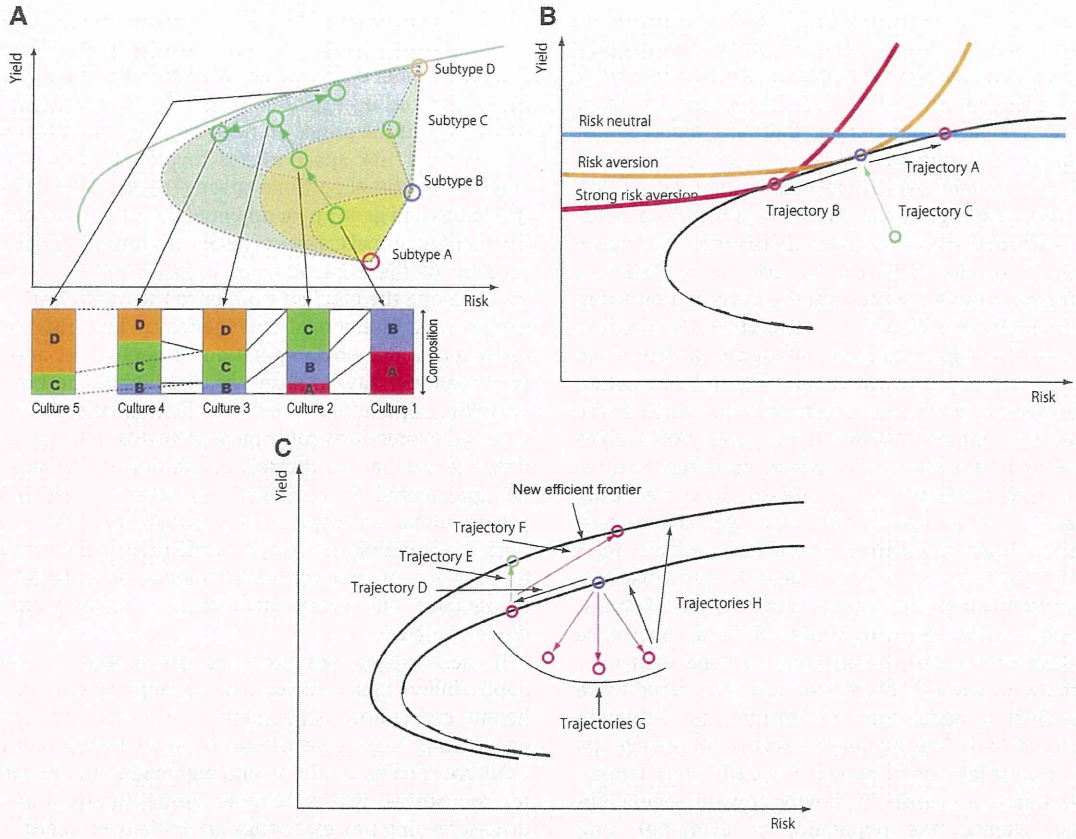

Figure 4 (**A**) In biological application of portfolio selection, each individual is mapped on the yield–risk space. A culture of cells may contain multiple different subtypes with mutations and epigenetic modifications. Assume a culture of cells (or organisms) composed of subtypes A, B, C, and D. At the initial stage, A and B may be dominant and C and D may be negligible (Culture 1). However, subtype C better fits the environment and grows faster than A and B (Culture 2). Subtype D starts to grow faster than the others and changes the subtype composition of the culture (Culture 3). At this stage, the composition of the culture may be sufficiently optimized for the given culture condition. Suppose the culture condition is changed now to have greater perturbations. Subtype D may not be able to tolerate it and will decrease the rate of proliferation and may even reduce in number, and subtype C may grow faster than the other subtypes (Culture 4). Alternatively, subtype D may continue to grow faster than other subtypes if the environment becomes even more stable. (**B**) A population of cells may evolve toward the efficient frontier. Under the risk-aversion indifference curve, the population arrives at the blue circle on the efficient frontier. The risk-aversion curve represents cases in which higher-level perturbations are imposed on the culture compared with a risk-neutral case. Under the stable condition in which selection pressures other than growth speed are not significant, the risk-neutral indifference curve is likely to be applied. The population follows Trajectory A and maximizes its growth rate at the cost of robustness. Imposing a higher level of perturbation may result in transition of the state through Trajectory B. (**C**) Cost-free resistance may be a result of taking Trajectory E or F to a new efficient frontier. There may be cases in which the population moves back to suboptimal regions (Trajectories G). Chemotherapy for cancer may shift the point inside the efficient frontier with different end points because of heterogeneous subpopulations. However, tumor cells may again evolve to gain proliferation potential despite the presence of anticancer drugs (Trajectories H). Tumor cells that undergo this transition may be too optimized for this specific therapeutic intervention, which implies possible efficacy when therapeutic regimens are switched. This may explain the collateral sensitivity of drug resistance tumor cells (Skipper *et al*, 1972).

involve genes related to adaptations to environmental changes, it is likely that the projected position of *B. subtilis* is on the efficient frontier and optimized for the risk-aversion indifference curve (orange line in Figure 4B), because any change to increase biomass would be associated with an increased risk under environmental fluctuations (Trajectory A in Figure 4B). Thus, although Fischer and Sauer argue that *B. subtilis* exhibits suboptimal metabolism, it can be considered optimal for the risk-aversion indifference curve.

Culturing microorganisms or cells under a chemo-static laboratory setup may enable the creation of an almost perturbation-free environment, unless explicitly imposed. In such a case, a risk-neutral indifference curve can be applied to determine the optimal portfolio (blue line in Figure 4B). For example, a population of *E. coli* evolved in the laboratory may quickly arrive at one of the projected positions on the efficient frontier and move along the trajectory of maximum biomass production through evolution (Ibarra *et al*, 2002) (Trajectory A in Figure 4B). The line of optimality in the phenotype phase plane as shown in Ibarra *et al* (2002) may correspond to the efficient frontier under stationary condition. In fact, their Figure 4 shows that the yield of bacteria evolves toward the line of optimality that is consistent with Figure 3 (A–C) in this paper. qIt should be noted that the line of optimality does not reflect the risk factor against perturbations. It only illustrates yield optimization. Therefore, it can be speculated that the *E. coli* that achieved maximum biomass production is more fragile against environmental change than those that have not evolved.

Interestingly, there are studies reporting that some pathogens evolve to overcome decreased growth fitness. As a result,

they can become drug resistant and maintain a competitive growth rate (Andersson, 2006). Although there is controversy with regard to this concept of 'cost-free evolution,' if it is correct, this compensatory evolution is thought to adapt to drugs that result in individuals that are more robust against drug insults, without increasing fragility elsewhere or undermining system performance measured by growth rate. In general, pathogens that have acquired drug resistance are known to have less growth fitness than pathogens without drug resistance. This can be seen as a trajectory along the efficient frontier, but toward the lower-left direction in Figure 4B (Trajectory B) and 4C (Trajectory D). Because of the existence of a drug, pathogens that are able to proliferate under drug exposure grow faster than others. Such pathogens may arise because of random mutations that better fit the drug-exposed environment. As a result, the population evolves to be optimal under the strong risk-averse indifference curve. This implies that trade-offs exist between increased drug resistance and a competitive growth rate against nonresistant pathogens. Again, 'robustness' is used as a general term to define the organism's tolerance against perturbations, including environmental fluctuations, the addition of drugs, and mutations. Although acquisition of drug resistance does not affect an organism's capability to cope with non-drug perturbations, overall robustness was considered to be increased because of added tolerance to the drug. Although the existence of 'cost-free evolution' seems to breach the concepts of robustness–performance trade-off, it is consistent because this is a process of moving toward a new efficient frontier (hence, the population is evolving), and robustness–performance trade-off can be observed only on the efficient frontier. The efficient frontier has changed because of the presence of a drug that was not a factor in determining the original efficient frontier (Trajectory E or F in Figure 4C).

Predictions and implications

The application of the concept of portfolio selection to biological systems results in testable predictions. First, it is predicted that the growth rate or biomass production of organisms and cells can be improved through evolution without increasing fragility until the efficient frontier is reached. A trade-off emerges only at the efficient frontier. This can be tested by random sampling of cells in artificial evolution experiments under a stationary culture condition, as shown in Figure 3. By the same token, the growth rate or biomass production of a population of organisms and cells can be improved without increasing their fragility against perturbations. Only when the population is on the efficient frontier do changes in yield and risk affect each other, hence a trade-off emerges. Therefore, robustness (or fragility) is not always conserved; it is conserved only when the system is on the efficient frontier.

Second, once the population or individual cells are on the efficient frontier and a stable culture condition persists, their position in the yield–risk space may move along the efficient frontier to the right for higher yield at the cost of robustness. This is because of the higher growth rate of a subtype over others that better fit the condition. Whether the population is on a trajectory toward the efficient frontier or moving along the efficient frontier can be distinguished by looking at the types of mutations and upregulation of genes that occur during such transitions. If the projected position of the population of cells on the yield–risk space moves toward the efficient frontier from a suboptimal portfolio space (Trajectory C in Figure 4B), mutations and gene up- or downregulations can be observed in broader functional classes of genes. In contrast, if the projected position of the population of cells on the yield–risk space moves along the efficient frontier to the right (Trajectory A in Figure 4B), mutations that generate high-risk high-yield phenotypes and downregulation of genes that accounts for perturbations may be observed. Prediction can be tested by sampling populations of cell and individual cells for sequencing and expression profile measurements to identify distribution of genes that are affected. In addition, different genes may be upregulated in a culture condition in which multiple perturbations are constantly imposed, because this would push the population to a lower-yield projected position. Genes that are accountable for environmental perturbations will be upregulated and genes that attain a higher yield may be downregulated.

If these conjectures hold and are proven to have wider applicability, there will be several implications for how we handle cell culture experiments. Cells cultured for multiple generations may have the problem of being optimized for a culture-specific condition and higher growth rate rather than for robustness against broader perturbations. Consider the drug-screening process. Drugs are initially screened using cell cultures. When a cancer cell line is used, for example, various drug candidates are applied for various cell lines. Cells in the culture are those that best fit the specific culture condition, which does not necessarily represent an *in vivo* environment for tumor cells. The most successful drug candidate may then be the one that undermines the growth of cells that are optimized for this specific condition. As *in vivo* cancer cells may be optimized for surviving under various perturbations, but may not for growth rate, a serious discrepancy exists between cells used for screening and actual cancer cells. Such a discrepancy may be mitigated if a culture condition can be set to impose various perturbations mimicking the cancer cells to which the body may be exposed. Thus, a deeper understanding of the type of perturbations that tumor cells in the body may be exposed to may make it possible to develop a multiple perturbation culture system that may improve the screening process.

By the same token, induced stem cells that are screened for therapeutic purposes may entail a similar problem. Cells with undermined robustness may be selected in favor of efficient reprogramming and upregulation of induction and differentiation markers, rather than cells that maintain robustness against broader perturbations. Currently, multiple generations are required for induction of pluripotent stem cells and elimination of epigenetic traces that are reminiscent of original cells (Masaki *et al*, 2007). During this process, which often requires multiple passages, new epigenetic modifications that are introduced by specific culture conditions are inevitable (Rubin, 1994; Meissner *et al*, 2008). It remains to be seen whether characteristics coselected for

high-yield subtypes entail any unwanted characteristics for therapeutic use.

With the introduction of the portfolio selection concept, observed breaches of trade-offs and enigma of performance suboptimality can be explained. Further studies and verifications are expected to lead to solid theories for biological systems and their applications to medical research.

Supplementary information

Supplementary information is available at the *Molecular Systems Biology* website (http://www.nature.com/msb).

Conflict of interest

The author declares that he has no conflict of interest.

References

Andersson DI (2006) The biological cost of mutational antibiotic resistance: any practical conclusions? *Curr Opin Microbiol* **9:** 461–465

Bode H (1945) *Network Analysis and Feedback Amplifier Design.* Melbourne, FL: Krieger

Carlson JM, Doyle J (1999) Highly optimized tolerance: a mechanism for power laws in designed systems. *Phys Rev E Stat Phys Plasmas Fluids Relat Interdiscip Topics* **60** (2 Pt A): 1412–1427

Csete ME, Doyle JC (2002) Reverse engineering of biological complexity. *Science* **295:** 1664–1669

Fell D (1997) *Understanding the Control of Metabolism.* London: Portland Press

Fischer E, Sauer U (2005) Large-scale *in vivo* flux analysis shows rigidity and suboptimal performance of Bacillus subtilis metabolism. *Nat Genet* **37:** 636–640

Ibarra RU, Edwards JS, Palsson BO (2002) Escherichia coli K-12 undergoes adaptive evolution to achieve in silico predicted optimal growth. *Nature* **420:** 186–189

Kitano H (2004) Biological robustness. *Nat Rev Genet* **5:** 826–837

Kitano H (2007) Towards a theory of biological robustness. *Mol Syst Biol* **3:** 137

Markowitz H (1991) *Portfolio Selection: Efficient Diversification of Investments.* Hoboken, NJ: John Wiley & Sons

Masaki H, Ishikawa T, Takahashi S, Okumura M, Sakai N, Haga M, Kominami K, Migita H, McDonald F, Shimada F, Sakurada K (2007) Heterogeneity of pluripotent marker gene expression in colonies generated in human iPS cell induction culture. *Stem Cell Res* **1:** 105–115

Meissner A, Mikkelsen TS, Gu H, Wernig M, Hanna J, Sivachenko A, Zhang X, Bernstein BE, Nusbaum C, Jaffe DB, Gnirke A, Jaenisch R, Lander ES (2008) Genome-scale DNA methylation maps of pluripotent and differentiated cells. *Nature* **454:** 766–770

Pareto V (1935) *The Mind and Society (English version).* New York: Dover

Reynolds D, Carlson JM, Doyle J (2002) Design degrees of freedom and mechanisms for complexity. *Phys Rev E Stat Nonlin Soft Matter Phys* **66** (1 Pt 2): 016108

Rubin H (1994) Cellular epigenetics: control of the size, shape, and spatial distribution of transformed foci by interactions between the transformed and nontransformed cells. *Proc Natl Acad Sci USA* **91:** 1039–1043

Skipper HE, Hutchison DJ, Schabel Jr FM, Schmidt LH, Goldin A, Brockman RW, Venditti JM, Wodinsky I (1972) A quick reference chart on cross resistance between anticancer patients. *Cancer Chemother Rep* **56:** 493–498

Stelling J, Klamt S, Bettenbrock K, Schuster S, Gilles ED (2002) Metabolic network structure determines key aspects of functionality and regulation. *Nature* **420:** 190–193

OPEN ACCESS Freely available online PLoS COMPUTATIONAL BIOLOGY

Large-Scale Analysis of Network Bistability for Human Cancers

Tetsuya Shiraishi[1]*, Shinako Matsuyama[2], Hiroaki Kitano[1,3,4]

1 Sony Computer Science Laboratories, Shinagawa-ku, Tokyo, Japan, **2** Sony Corporation, Shinagawa-ku, Tokyo, Japan, **3** The Systems Biology Institute, Shinjuku-ku, Tokyo, Japan, **4** Okinawa Institute of Science and Technology, Kunigami, Okinawa, Japan

Abstract

Protein–protein interaction and gene regulatory networks are likely to be locked in a state corresponding to a disease by the behavior of one or more bistable circuits exhibiting switch-like behavior. Sets of genes could be over-expressed or repressed when anomalies due to disease appear, and the circuits responsible for this over- or under-expression might persist for as long as the disease state continues. This paper shows how a large-scale analysis of network bistability for various human cancers can identify genes that can potentially serve as drug targets or diagnosis biomarkers.

Citation: Shiraishi T, Matsuyama S, Kitano H (2010) Large-Scale Analysis of Network Bistability for Human Cancers. PLoS Comput Biol 6(7): e1000851. doi:10.1371/journal.pcbi.1000851

Editor: Nathan D. Price, University of Illinois at Urbana-Champaign, United States of America

Received May 14, 2009; **Accepted** June 3, 2010; **Published** July 8, 2010

Funding: The authors received no specific funding for this work.

Competing Interests: The authors have declared that no competing interests exist.

* E-mail: Tetsuya.Shiraishi@jp.sony.com

Introduction

Understanding diseases within the context of biological networks is one of the major challenges in systems biology. Diseases often persist and resist therapeutic intervention. The persistence of a disease in a system must be reflected in the ability of the system's networks to maintain the state underlying the disease. In other words, networks are "locked-in" to disease states and maintain their stability. Thus, it is important to understand how such multi-stable states are achieved within the context of network topology and to understand the dynamics of these states. A network robust against a range of perturbations can maintain a healthy state but can also, when affected by a disease, transition to a new steady state that is often also robust against perturbations, making the disease state persistent. A series of disease progressions may be the result of a sequence of state transitions in the network dynamics (Fig. 1A). Bistable circuits may drive such transitions and are thus critical in enabling the initiation and progression of diseases to be understood (Fig. 1 B).

Complex networks exhibiting such multi-stability must have a set of bi-stable or multi-stable circuits consisting of proteins and genes. The identification of circuits that exhibit bi- or multi-stability within large protein-interaction and gene-regulation networks would provide information useful for understanding the mechanism(s) of network bistability. Furthermore, circuits exhibiting bistability can be potential drug targets or biomarkers for classifying disease states.

Network dynamics are regulated by the structure of the network and the flow of information through feedforward and feedback loops. Mutual activation or mutual inhibition configurations can maintain the flow of biological information between two molecules and act as network memories or switches. Furthermore, an activation-inhibition configuration, in which one molecule stimulates the other while the latter inhibits the former, generates dynamics with periodicity like that seen in circadian rhythms and cell cycles [1]. The stability and characteristics of Boolean networks comprising these configurations were studied in detail by Kauffman et al. [2]. In the study reported here, we focused on mutual inhibition, which is thought to be involved in the stable deviations of a system observed during the progression of tissue from a normal to a diseased state.

There are several important network motifs for system configurations [3–6] in protein-protein networks. One of them, a toggle switch that converts a continuous input signal into a discontinuous ON or OFF response, plays a fundamental role in information processing and decision making. Among the naturally occurring toggle switches that have been reported are the lambda phage lysis–lysogeny switch [7–9], switches in the lactose operon repressor system [10–12], the mitogen-activated protein kinase (MAPK) cascade [13–20], the Sonic hedgehog network in stem-cell differentiation [21], cell-cycle regulatory circuits [22–24], and the rapid lateral propagation of receptor tyrosine kinase activation [25]. Genetically engineered toggle switches have been constructed experimentally in Escherichia coli [26,27] and in mammalian cells [28].

A robust toggle switch behaves as a signal memory unit by using a hysteresis mechanism [29]. Once in the ON state, a toggle switch remains in the ON state even if the stimulus concentration falls below the threshold level [11,13,23,24,30,31]. A molecular network's persistence in a disease state might be due to the hysteresis of toggle switches.

To identify circuits exhibiting bi- and multi-stability, we topologically analyzed activation and inhibition in proteins on a large scale by using various databases containing expression array data for various diseases. We compared the progression stages of these diseases with those of control samples by using data for healthy individuals taken from available databases, and we identified sets of switch circuits possibly responsible for maintaining the persistent disease states by using network topologies to analyze that data.

Author Summary

Since most disease states exhibit a certain level of resilience against therapeutic interventions, each disease state can be considered to be homeostatic to some extent. There must be one or more mechanisms that cause the gene-regulatory network to maintain a certain state, and one such mechanism is a bistable switch. In this work, bistable switch networks were constructed and their ON(upregulated)/OFF(downregulated) states were compared between human cancers and healthy control samples. Changes in the ON/OFF state with the progression of cancer were demonstrated. A series of genes that might serve as a drug target or diagnosis biomarker was identified. The approach presented here should provide useful insights into the states of biological networks, which may lead to the discovery of novel drug targets and therapeutic interventions.

Results

Extraction of bistable toggle switches

There are theoretically many system configurations that can lead to bistability [18,32–35]. We focused on bistable toggle switches (BTSs) with double-negative feedback. Such switches can be constructed from any two genes that mutually repress their expression. We considered three types of network motifs that can exhibit bistable behavior (Fig. 2).

1. Type-1 BTS: A type-1 BTS uses a basic motif that has been identified in E. coli [26] and has mutually inhibitory interaction and positive autoregulators. In a circuit with a double-negative feedback loop, proteins A and protein B inhibit or repress each other. Positive autoregulation is a type of feedback in which proteins directly activate the transcription of their own genes. Under the right circumstances, there could be a stable steady state in which A is "ON" and B is "OFF" or B is "ON" and A is "OFF." This bistability is maintained through positive autoregulation.
2. Type-2 BTS: Only a small number of transcription factors with a positive autoregulation ability have been reported. From the viewpoint of dynamic properties, positive autoregulation has the same functional meaning that a positive feedback loop (double-positive feedback or double-negative feedback) does [36]. We thus defined two mutually inhibitory nodes with a positive feedback loop between them as a type-2 BTS.
3. Type-3 BTS: A theoretical study of modeling genetic switches with positive feedback loops [37] revealed that mutual inhibition is maintained even if a molecule that signals information intervenes between the molecules constituting a switch. We defined two nodes that inhibit each other through other genes (mediators) as a type-3 BTS. Although it is theoretically possible that a positive feedback loop can be formed even if the intervening molecules are identical, in the present study we excluded this possibility.

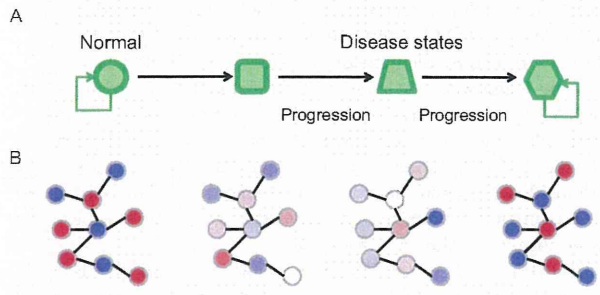

Figure 1. State transitions in network dynamics and disease progression. A: A network in a healthy state is robust against a range of perturbations, so it can continue to maintain a healthy state. With the onset of a disease, however, the network transitions to a new steady state that is also often robust against perturbations, making the disease state persistent. B: These state transitions might be driven by bistable switch networks. The nodes represent genes and the edges between them represent the pairing of bistable toggle switches. Red and blue nodes correspond to ON (upregulated) and OFF (downregulated) states.
doi:10.1371/journal.pcbi.1000851.g001

It is possible that double-negative feedback can be a bistable toggle switch when both nodes have positive feedback loops. Two BTSs can share their mutual inhibition configurations as positive feedback loops and can form network configurations.

Next, bistable toggle switches defined above was extracted from large-scale databases (ResNet 3.0, Ariadne Genomics Inc.) containing data for interaction networks. We detected 6585 pairs of bistable toggle switches, and these switch nodes formed a large network. Four-hundred and forty-two genes are involved in these BTS pairs, and the hubs of switch nodes in the network are clearly visible because of their high degree of connectivity (Fig. 3). A complete list of the BTS pairs is provided in Protocol S1, and a Cytoscape session file is provided in Protocol S2. It should be noted that this network was constructed using text mining and that the molecular details of each interaction were not verified. It is nevertheless a reasonable starting point, and whether or not a listed BTS actually exhibits bistability can be further examined using microarray data.

Tests using mRNA microarray data

ArrayExpress microarray data were used to further examine the states of the BTS pairs. It is obvious that a BTS has four possible states: "ON/ON," "ON/OFF," "OFF/ON," and "OFF/OFF." Mathematical analysis of bistability for the chosen parameter condition demonstrated that the probability of "ON/OFF" and "OFF/ON" states is high, that of "ON/ON" is low, and that of "OFF/OFF" is extremely low [38]. This is the reason we focused on the BTSs that demonstrated "ON/OFF" or "OFF/ON" states.

The ArrayExpress experimental categories and the mean number of corresponding BTS pairs with a significant ON/OFF change are shown in Fig. 4. In the set of 6585 candidate BTSs the number of pairs with a significant ON/OFF change ranged from 0 to 1927 (mean = 298.6), while in a set of 6585 randomly selected gene pairs the number of pairs with a significant ON/OFF change ranged from 0 to 273 (mean = 72.1).

The switching of a molecule's function to the ON state generally means the molecule's intrinsic function related to intracellular molecular systems has become stronger, whereas switching to the OFF state means it has become weaker. The ON state of a molecule is produced not only by an increase in the absolute amount of that molecule but also by actions such as activation due to phosphorylation-induced transformation of the molecule's three-dimensional structure or to translocation of the molecule to an location where it can carry out its function properly.

In these studies using mRNA expression data from microarrays, the toggling of a BTS pair was defined as an instance in which a sample's mRNA level for one of that pair's molecules increased (relative to a control) and the mRNA level for the other of that pair's molecule decreased (relative to the same control).

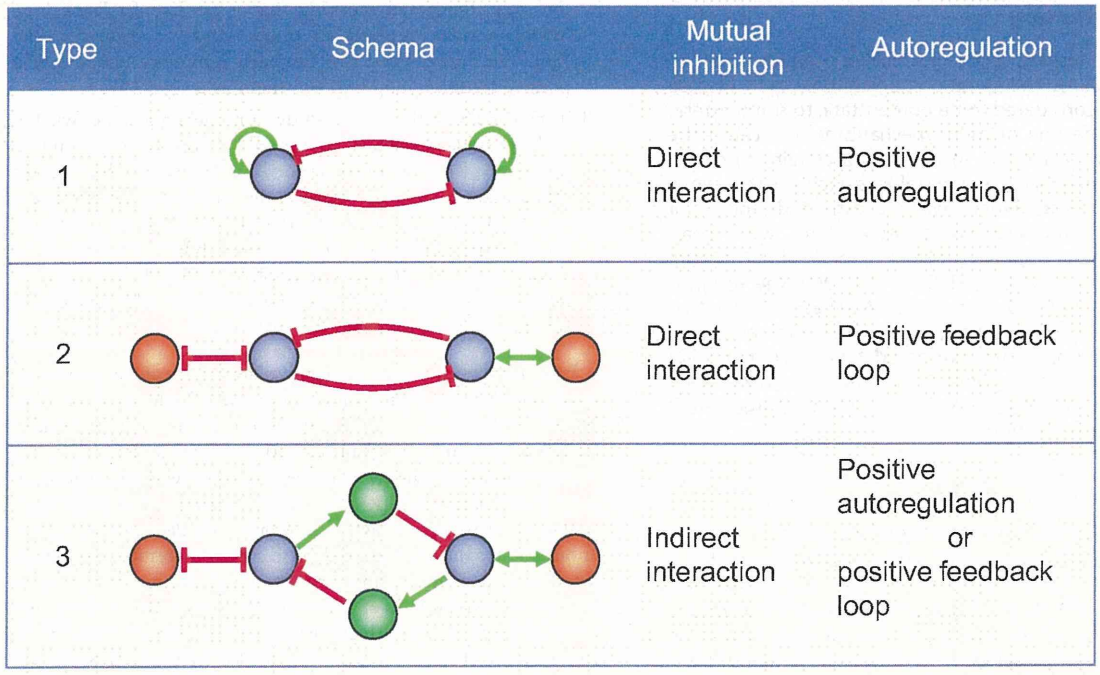

Figure 2. Motifs of bistable toggle switches. A type-1 bistable toggle switch (BTS) contains two genes with positive autoregulation. Each gene mutually inhibits the other's expression. The two genes in the type-2 BTS also suppress each other's expression. Each gene has double positive or negative feedback with the other gene, so the same function as a type-1 BTS may be exhibited. A type-3 BTS was constructed on the basis of a theoretical study on the modeling of genetic switches with positive feedback loops. The blue, green, and orange nodes respectively correspond to switch genes, mediators, and genes constituting a feedback loop. Positive (upregulated) interactions are indicated by green lines and negative (downregulated) interactions are indicated by red lines.
doi:10.1371/journal.pcbi.1000851.g002

A notable finding is that when mRNA levels were compared between induced pluripotent stem (iPS) cells and donor controls, more than 1000 BTS pairs demonstrated significant changes in the ON/OFF states. The high frequency of these changes in iPS cells is reasonable in that an iPS cell is in an undifferentiated state committed to differentiation to a particular lineage, in which many BTSs might be involved [39]. iPS cells have been generated from mouse and human somatic cells by using retroviruses or lentiviruses to introduce Oct3/4 and Sox2 with either Klf4 and c-Myc or Nanog and Lin28 [40]. These factors have been reported to result in bistability when they combine with other factors and form mutual-activation and mutual-inhibition motifs [41–43].

Lung cancer

Lung cancer is the leading cause of cancer-related deaths [44], and tobacco smoking is the strongest etiological factor associated with lung cancer. Prior studies have demonstrated that smoking creates a field of molecular injury throughout the airway epithelium exposed to cigarette smoke [45].

Figure 5A depicts the toggling of BTS ON/OFF states inferred from time-dependent data (ArrayExpress ID: E-GEOD-10700 and E-GEOD-10718) for the mRNA expression in normal human bronchial epithelial cells exposed to cigarette smoke for 24 hours. Toggling began at 2 hours (Fig. 5B) and was observed most frequently at 4 hours (Fig. 5C). SOCS3 (suppressor of cytokine signaling 3) was observed early, while BTSs related to HMOX1 (heme oxygenase 1), CSF2 (colony stimulating factor 2), and SPP1 (secreted phosphoprotein 1) were observed throughout the 24-h period.

SOCS3 inhibits cytokine signaling via the JAK(Janus kinase)/STAT(signal transducers and activators of transcription) pathway. Recent research has demonstrated that the activation of SOCS3 in the lung occurs during the acute inflammatory response [46]. Frequent hypermethylation in the CpG islands of the functional SOCS3 promoter has been found in lung-cancer tissue samples to correlate with its transcription silencing [47]. The OFF states of EGF (epidermal growth factor) and MAPK8 (mitogen-activated protein kinase 8) were linked to the ON states of CSF2 and HMOX1, which became the main players at four or more hours of exposure. CSF2 and HMOX1 were connected through several genes in the OFF state, including IL13 (interleukin 13), IFNG (interferon gamma), and FN1 (fibronectin 1), which are related to inflammatory responses and wound healing.

Figure 6 illustrates the state of BTS toggling for a comparison of mRNA expression (ArrayExpress ID: E-GEOD-10072) in non-small cell lung carcinoma (NSCLC) patients with a history of smoking (Fig. 6A) along with those currently smoking (Fig. 6B) with mRNA expression seen in normal lung tissue. The bold black frames surround molecules that are also in the BTS molecules whose toggling is shown in Fig. 5A.

ON/OFF patterns of FN1-SPP1 (Fig. 6A) and IGF1-SPP1 (Fig. 6B) were observed in the data gathered in experiments exposing normal human bronchial epithelial cells to cigarette smoke. SPP1 is a secreted integrin-binding glycoprotein that is overexpressed in various tumors and has been reported to be involved in tumorigenesis and metastasis. High expression of SPP1 is a significantly unfavorable prognostic factor for the survival of patients with NSCLC [48].

In addition, although some EDN1(endothelin-1)-related BTS pairs and SHC1(Src homology 2 domain containing transforming protein)-related BTS pairs are shared in lung cancer tissue in current and former smokers, a considerable number of differing

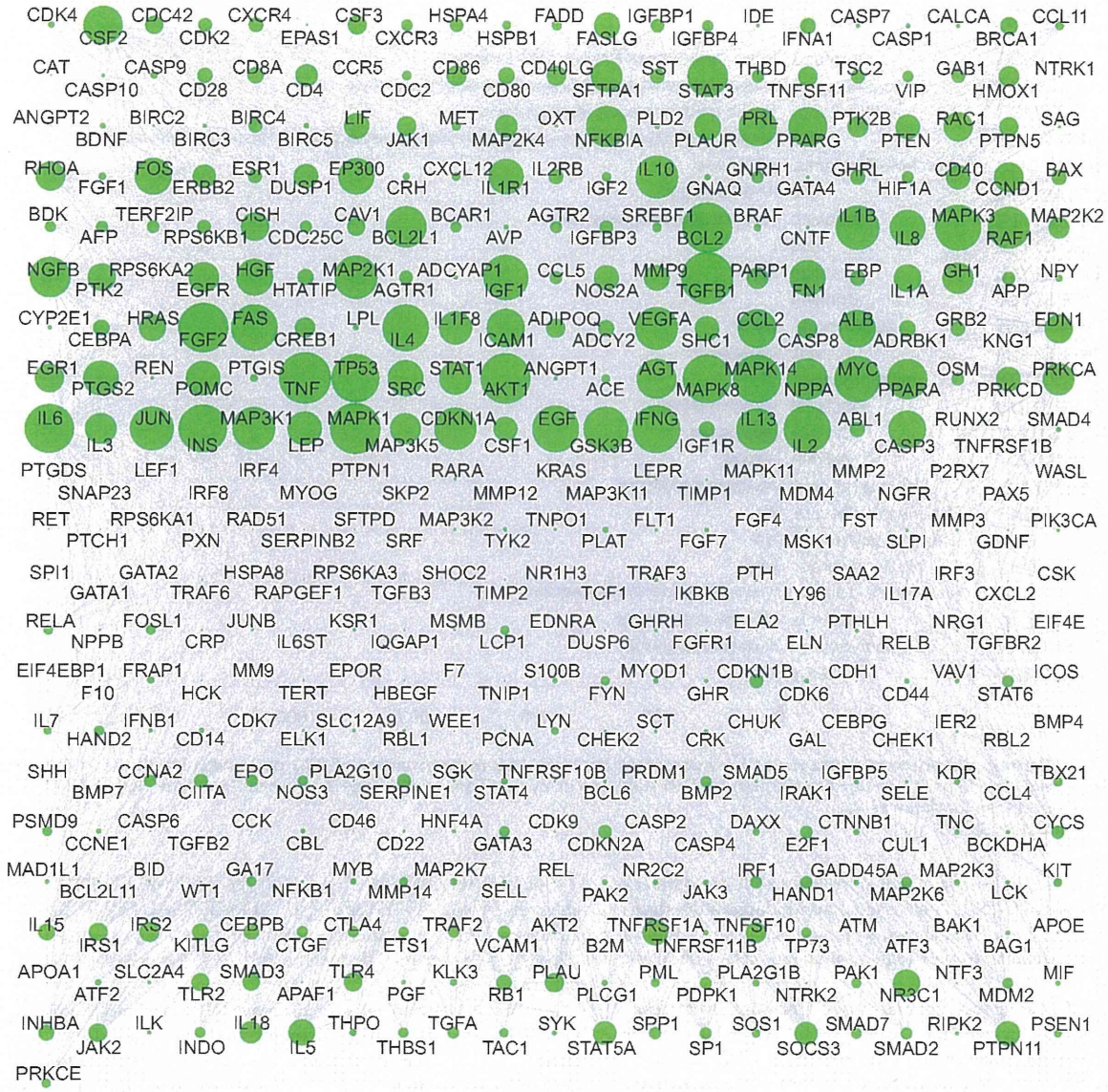

Figure 3. Cytoscape visualization of network composed of bistable toggle switch pairs. Four-hundred and forty-two genes are involved in 6585 bistable toggle switch pairs. Nodes are shown in sizes proportional to their connectivity, making the hubs of switch nodes clearly visible. The Cytoscape session file for this network is available in Protocol S2.
doi:10.1371/journal.pcbi.1000851.g003

patterns are evident. This suggests that the mechanisms for carcinogenesis differ depending on the lengths of time that current and former smokers have smoked. EDN1, which is a hypoxia-inducible angiogenic growth factor for surrounding epithelial and endothelial cells, plays an important role in cancer-stromal interactions and tumor progression, and its expression is related to poor prognosis in NSCLC [49].

Small molecules that can put these BTS pairs into normal ON/OFF states might be useful in preventing the progression of lung cancer in both current and former smokers.

Hepatocellular carcinoma

Hepatocellular carcinoma (HCC) is a primary cancer that originates in hepatocytes and typically follows cirrhosis or chronic-hepatitis virus infections [50], and the most significant risk factors for HCC are chronic infections with either hepatitis B virus or hepatitis C virus (HCV).

Figure 7 is a BTS toggling graph in which mRNA expression data (ArrayExpress ID: E-GEOD-6764, [51]) for tissues from patients with HCV-induced dysplasia and HCC are compared with mRNA expression data for normal liver tissue. The molecules surrounded by bold lines are BTSs for which toggling was observed when comparing dysplastic liver tissue (cirrhotic tissue and dysplastic nodules), a precursor of liver cancer, with normal liver tissue. The two tissue types share many BTSs associated with PTGS2 (prostaglandin-endoperoxide synthase 2; COX-2) and IL1B (interleukin 1, beta). It has been demonstrated that the expression pattern of PTGS2, a key enzyme of the

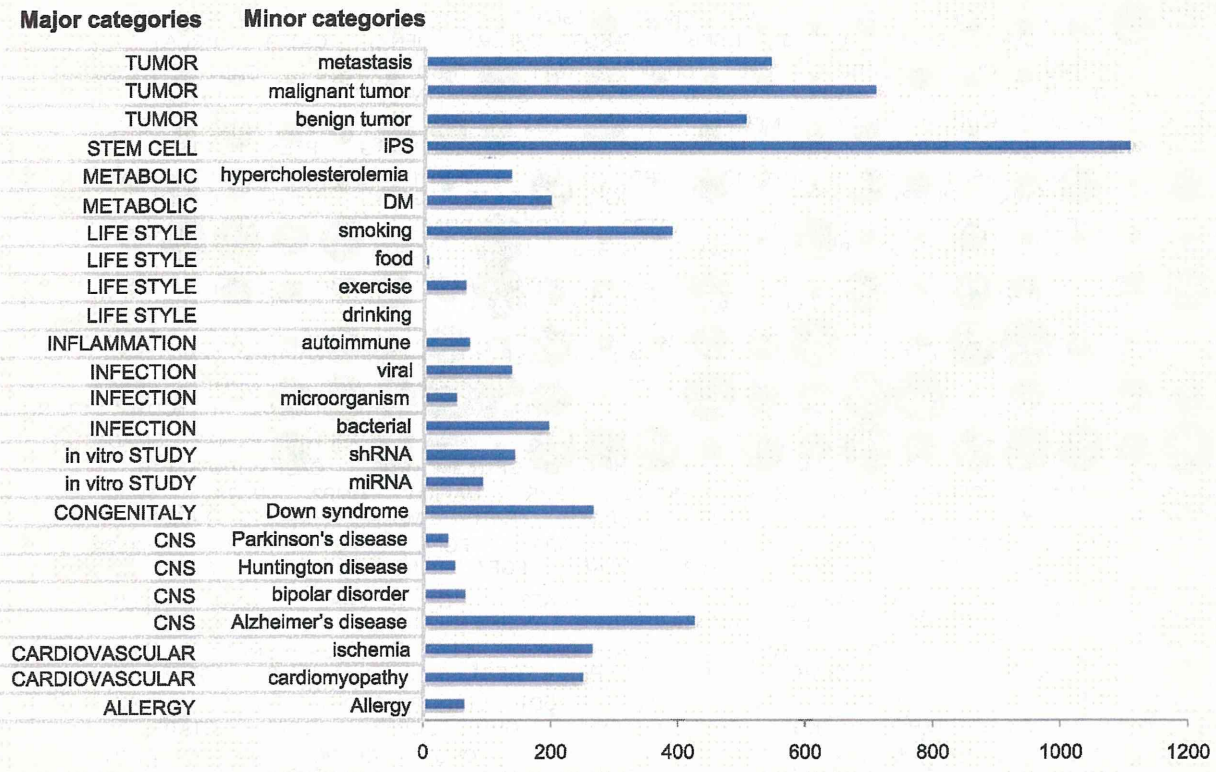

Figure 4. ArrayExpress experimental categories for microarray datasets and mean number of BTS pairs with significant ON/OFF change. There were few BTS pairs with significant changes for "lifestyle" and many with significant changes for "cancer." Note the higher number of BTS pairs for iPS cells than for donor cells.
doi:10.1371/journal.pcbi.1000851.g004

prostaglandin metabolism, is closely correlated with the differentiation grade of HCC [52]. Nonsteroidal anti-inflammatory drugs targeting PTGS2 have been shown to inhibit the proliferation of cultured hepatocellular cancer cells by inducing cell-cycle arrest [53].

When HCC tissue was compared with healthy liver tissue, toggling was most evident for CCNA2(cyclin A2)–related BTSs (Fig. 7) We therefore analyzed how the toggling of CCNA2-related BTSs rippled out to other BTS pairs during the malignant transition of HCC (Fig. 8).

CCNA2 activates CDC2 or CDK2 kinases and regulates the cell cycle positively by promoting G1/S and G2/M transitions in both the G1 and G2 phases of the cell cycle [54], while EGR1 (early growth response gene 1) has suppresses transformation [55]. The upregulation of CCNA2 and downregulation of EGR1 might thus play a key role in the dysregulation of normal growth in HCC carcinogenesis [56]. The downregulation of IL6 (interleukin 6) is involved in dysregulation of the immune response in early carcinogenesis.

After the toggling of CCNA2-related BTSs but still in the early stage of carcinogenesis, the OFF state of IL6 is related to the ON states of PTK2 and SMAD3 (SMAD family member 3). PTK2 and SMAD3 play important roles in cell growth and the activation of intracellular signal transduction pathways, suggesting that cell proliferation might accelerate during this stage.

Toggling of PTK2(ON)-BCL2(OFF) was observed in advanced and very advanced stages. BCL2 (B-cell CLL/lymphoma 2) suppresses apoptosis, and the downregulation of BCL2 might be involved in the acceleration of apoptosis in cancer cells.

Notably, the ON/OFF state of the TP53-IGF1 BTS was changed from "OFF-OFF" to "ON(TP53)–OFF(IGF1)" in advanced HCC. And in very advanced HCC, almost all IGF1-related BTS pairs demonstrated "ON(other)–OFF(IGF1)" patterns.

In the very advanced stage, many IGF1(insulin-like growth factor-1)-related BTS pairs demonstrated significant ON/OFF changes. The liver is the main source of IGF1, and the development of HCC is accompanied by significantly reduced serum IGF1 levels [57]. The downregulation of IGF1 and upregulation of a set of another pair of genes might affect a wide variety of cellular functions.

Discussion

We constructed bistable switch networks, compared their ON/OFF states with those of control (healthy) samples, and found that their states changed with disease progression and differed between patient subtypes. Since most disease states exhibit a certain level of resilience against therapeutic intervention, each can be considered to be homeostatic to some extent. This homeostasis implies the robust status of a dynamical network and could not be maintained without mechanisms that drive a network to maintain a certain state. One such mechanism is a bistable switch, so we should look for sets of bistable switch circuits in large-scale protein interaction networks.

Our analysis revealed that BTS states change with disease progression, and the implications of this are far reaching. For example, it might be possible to prevent or delay disease

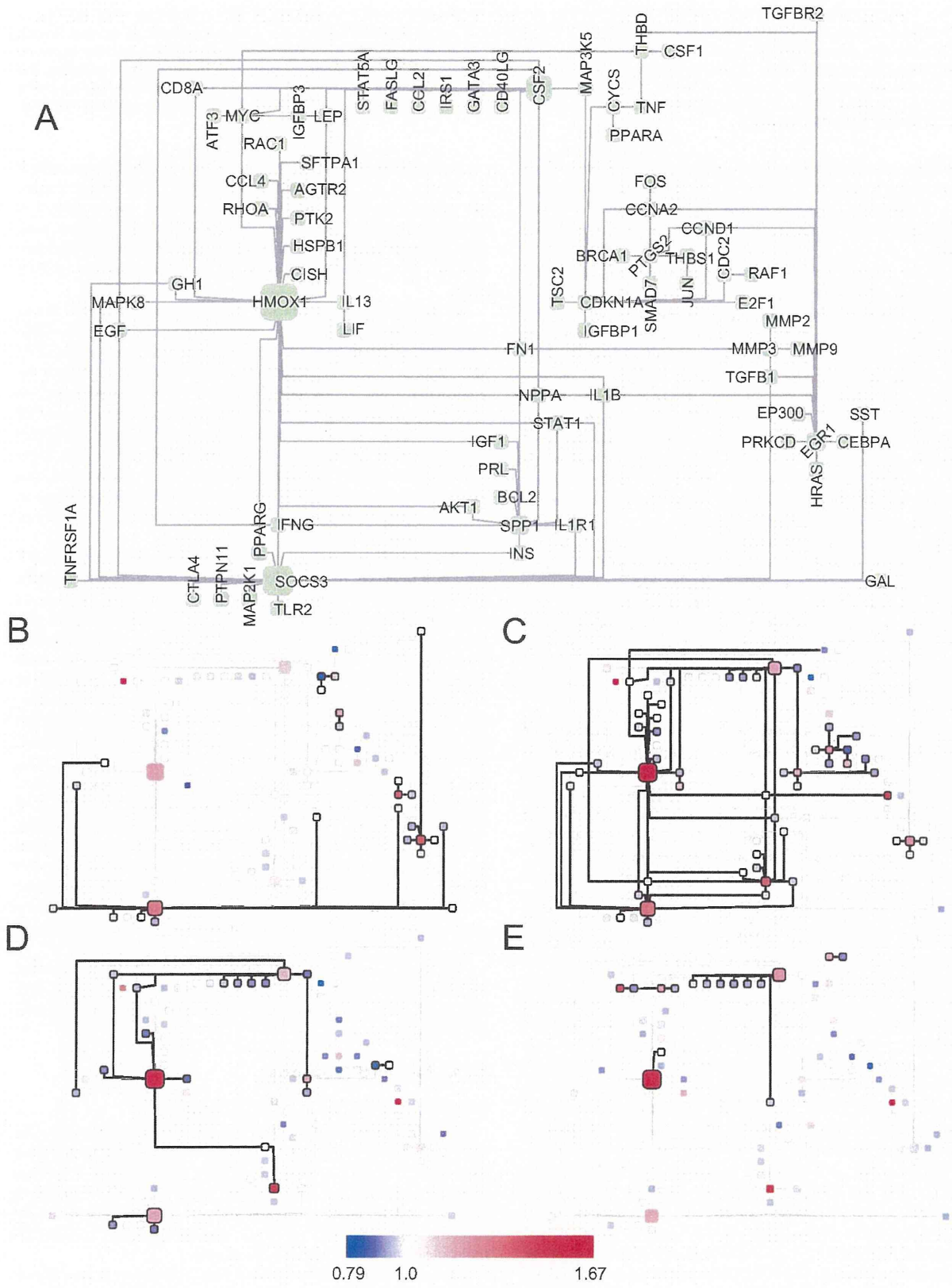
A
TGFBR2
THBD
CSF1
MAP3K5
STAT5A
FASLG
CCL2
IRS1
GATA3
CD40LG
CSF2
CD8A
CYCS
TNF
PPARA
ATF3
MYC
IGFBP3
LEP
RAC1
SFTPA1
CCL4
AGTR2
RHOA
PTK2
HSPB1
CISH
FOS
CCNA2
CCND1
BRCA1
PTGS2
THBS1
CDC2
RAF1
GH1
MAPK8
HMOX1
IL13
LIF
EGF
TSC2
CDKN1A
SMAD7
JUN
E2F1
IGFBP1
MMP2
FN1
MMP3
MMP9
TGFB1
NPPA
IL1B
STAT1
EP300
SST
IGF1
PRKCD
EGR1
CEBPA
PRL
HRAS
BCL2
AKT1
TNFRSF1A
PPARG
IFNG
SPP1
IL1R1
INS
CTLA4
PTPN11
MAP2K1
SOCS3
GAL
TLR2
B
C
D
E
0.79
1.0
1.67

Figure 5. Changes in ON/OFF states of BTSs for time series data for human normal bronchial epithelial cells exposed to smoke. A: Toggling inferred from time-dependent data (ArrayExpress ID: E-GEOD-10700 and E-GEOD-10718) for the mRNA expression of normal human bronchial epithelial cells exposed to cigarette smoke for 24 hours. B: 2 hrs after exposure start, C: 4 hrs after exposure start, D: 8 hrs after exposure start, E: 24 hrs after exposure start. The nodes represent genes and the edges between them represent the pairing of bistable toggle switches. The colors of nodes were automatically assigned as a continuous color gradient from red for ON (upregulated) to blue for OFF (downregulated) according to relative gene-expression levels of the nodes. In Figs. 4B–E, the BTS pairs framed by thick lines are pairs with significant toggling scores at that time.
doi:10.1371/journal.pcbi.1000851.g005

progression by perturbing one or more such switches. Such switches may be novel drug-target candidates for controlling disease progression. Analysis of the ON/OFF states of genes constituting bistable circuits revealed similarities between disease subtypes.

While our analysis has provided insightful information, it has shortcomings. First, the network topologies were based on commercial databases created using a text-mining system. This means that the details of the molecular interactions were not verified. The development of a more accurate interaction database would enable more precise and accurate analysis of bistable network behaviors and of the contributions of switch circuits to those behaviors. Second, the analysis was based solely on network topologies—no parametric features were considered. Although topological analysis enabled us to identify circuits exhibiting bistable behavior, whether circuits exhibiting bistable behavior apparently exhibit bistable behavior depends on the kinetic parameters associated with each interaction [58].

Using microarray data, we determined that the pairs of genes in the circuits we identified are polarized into ON and OFF states. Two mutually inhibitory nodes polarized into ON and OFF states do not function as a bistable switch if both genes are ON or OFF. This is why we focused on BTSs, which demonstrated "ON/OFF" or "OFF/ON" states. We should, however, note that the "ON/ON" states of some BTSs play important roles in mammalian embryogenesis [59], T-cell differentiation [60], and visual-system specification [61].

Cluster analysis of transcriptome data in microarrays is useful for classifying disease characteristics according to differences in expression patterns. Although several disease types that are difficult to classify morphologically have been classified using this approach, the rules underlying the cluster structure of the data are unclear, and the importance of each of the molecules in a cluster cannot be determined with a reasonable degree of certainty. The analysis of changes in gene-expression levels can also be used to create a list of molecules whose levels increase or decrease significantly over time or whose levels differ significantly between healthy and diseased tissues. Although examinations of gene interrelations using gene-ontology classification and analysis of the classification results using network diagrams have led to a greater degree of understanding of the changes in molecular networks, it is difficult to infer the meanings of biological interactions between molecules.

Our proposed method (i.e., focusing on BTS ON/OFF changes) takes as the starting point the interactions between molecules. This makes it easy to infer biological meaning and makes it possible to analyze time-dependent data for time periods corresponding to that of disease progression (from hours to years). In addition, while conventional methods sometimes neglect molecules that are downregulated, our method places equal importance on both increases and decreases in expression.

DNA microarray technology makes it possible to study the expression of thousands of genes at the same time, but much of the microarray data consists of low signal intensities that can produce erroneous gene expression ratios between control and experimental samples [62]. The distribution of the ratio of two random variables approaches a Cauchy, or Lorentzian, distribution, which has longer tails than Gaussian distributions [63,64]. In our results, far more BTS pairs had significant toggling scores than did random gene pairs, but a considerable number of random gene pairs did show significant ON/OFF changes. We should therefore consider the possibility of random error in the analysis of BTS pairs.

We used the transcriptome of normal tissue as the control in our analyses. This means that the identification of the molecular ON/OFF states inherent to normal tissue was unclear. Even if the ON/OFF state of a molecular pair for a certain switch is important for a particular tissue, if this state is retained in the diseased tissue, we would be unable to detect it in the present study because the ON and OFF states are not mutually exclusive. Therefore, molecules exhibiting even the slightest change are emphasized while those showing no change are ignored. We aim to overcome this drawback by identifying what types of ON/OFF changes occur in switches when embryonic stem (ES) cells or iPS cells undergo differentiation.

Since proteins are responsible for cell function, the ON/OFF state of a molecule must be determined at the protein level when searching for molecular-network structures mediating cell functions. Because there are more than 20 control steps along the way from mRNA to functional proteins [65], the reported expression levels of mRNA do not always agree with those of proteins—their translated products [66]. And even if there were a quantitative correlation between the levels of mRNA and functional protein, the efficiency of the translation process would be greatly affected by factors such as structural change and protein localization. Proteomics data for proteins in different cellular contexts is useful but is available for only some proteins. Transcriptome data analysis is the only method currently available for examining molecular networks on a large scale, but when testing the quality of BTS pairs in the future we will use all the relevant available data for the target proteins. Furthermore, to ensure bistability, the hysteresis phenomena must be confirmed when a perturbation has vanished. By conducting time-scale experiments in both directions when applying and removing perturbations, we should be able to further test the quality of BTS pairs.

Despite its shortcomings, the approach presented here provides useful insights into the states of biological networks, insights that may lead to discovery of novel drug targets and therapeutic interventions.

Materials and Methods

Preparation of basic interaction datasets

The lists of molecular interactions were constructed using the Ariadne Genomics ResNet human protein interaction database (ver. 3.0) compiled, using MedScan [67] natural language processing technology, from more than 13,000,000 PubMed abstracts and 43 publicly available full-text journals. The database contains data on over 200,000 objects (proteins and small molecules) and over 100,000 interactions.

The interactions can be divided into two major classes: direct physical interactions (binding, protein modifications, and promoter binding) and indirect regulatory interactions (regulation,

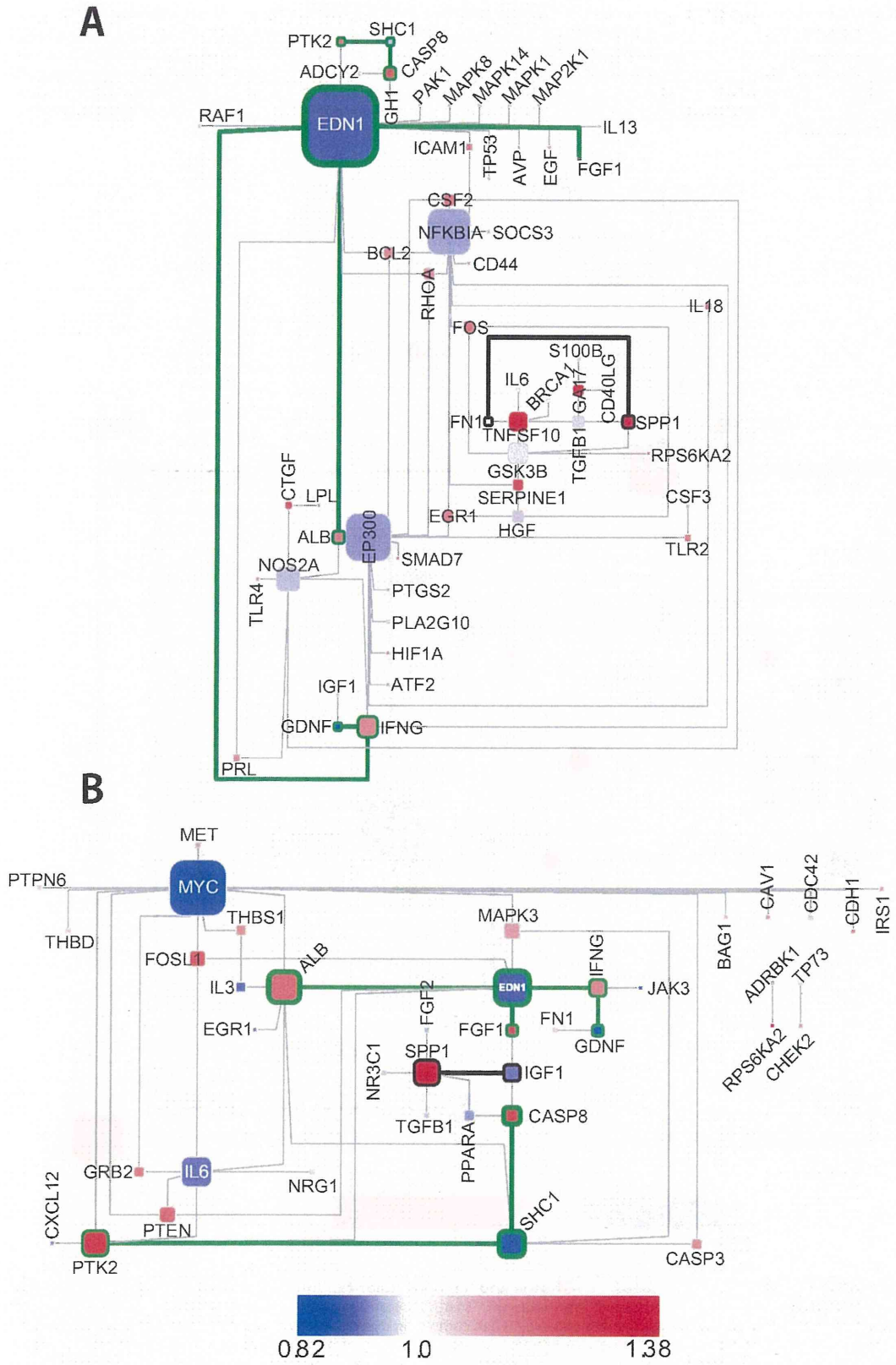
A
PTK2
SHC1
ADCY2
CASP8
GH1
PAK1
MAPK8
MAPK14
MAPK1
MAP2K1
RAF1
EDN1
IL13
ICAM1
TP53
AVP
EGF
FGF1
CSF2
NFKBIA
SOCS3
BCL2
CD44
RHOA
IL18
FOS
S100B
IL6
BRCA1
GA17
CD40LG
FN1
TNFSF10
SPP1
TGFB1
RPS6KA2
GSK3B
CTGF
LPL
SERPINE1
CSF3
EGR1
HGF
ALB
EP300
SMAD7
TLR2
NOS2A
TLR4
PTGS2
PLA2G10
HIF1A
IGF1
ATF2
GDNF
IFNG
PRL
B
MET
PTPN6
MYC
THBS1
MAPK3
CAV1
CDC42
CDH1
IRS1
THBD
FOSL1
ALB
IFNG
BAG1
IL3
EDN1
JAK3
ADRBK1
TP73
FGF2
FN1
EGR1
FGF1
GDNF
RPS6KA2
CHEK2
NR3C1
SPP1
IGF1
TGFB1
CASP8
PPARA
GRB2
IL6
NRG1
CXCL12
PTEN
SHC1
PTK2
CASP3
0.82
1.0
1.38

Figure 6. Changes in ON/OFF states of BTSs for lung cancer. The state of BTS toggling determined by comparing mRNA expression data (ArrayExpress ID: E-GEOD-10072) for normal lung tissue with that for lung-cancer patients with a history of smoking (former smokers) (Fig. 6A) and that for lung-cancer patients still smoking (current smokers) (Fig. 6B). The nodes and genes surrounded by bold black frames are those also shown in Fig. 5A. The nodes and edges surrounded by bold green frames are found in the former smokers as well as the current smokers. The nodes represent genes and the edges between them represent the pairing of bistable toggle switches. The colors of nodes were automatically assigned as a continuous color gradient from red for ON (upregulated) to blue for OFF (downregulated) according to relative gene-expression levels of the nodes.
doi:10.1371/journal.pcbi.1000851.g006

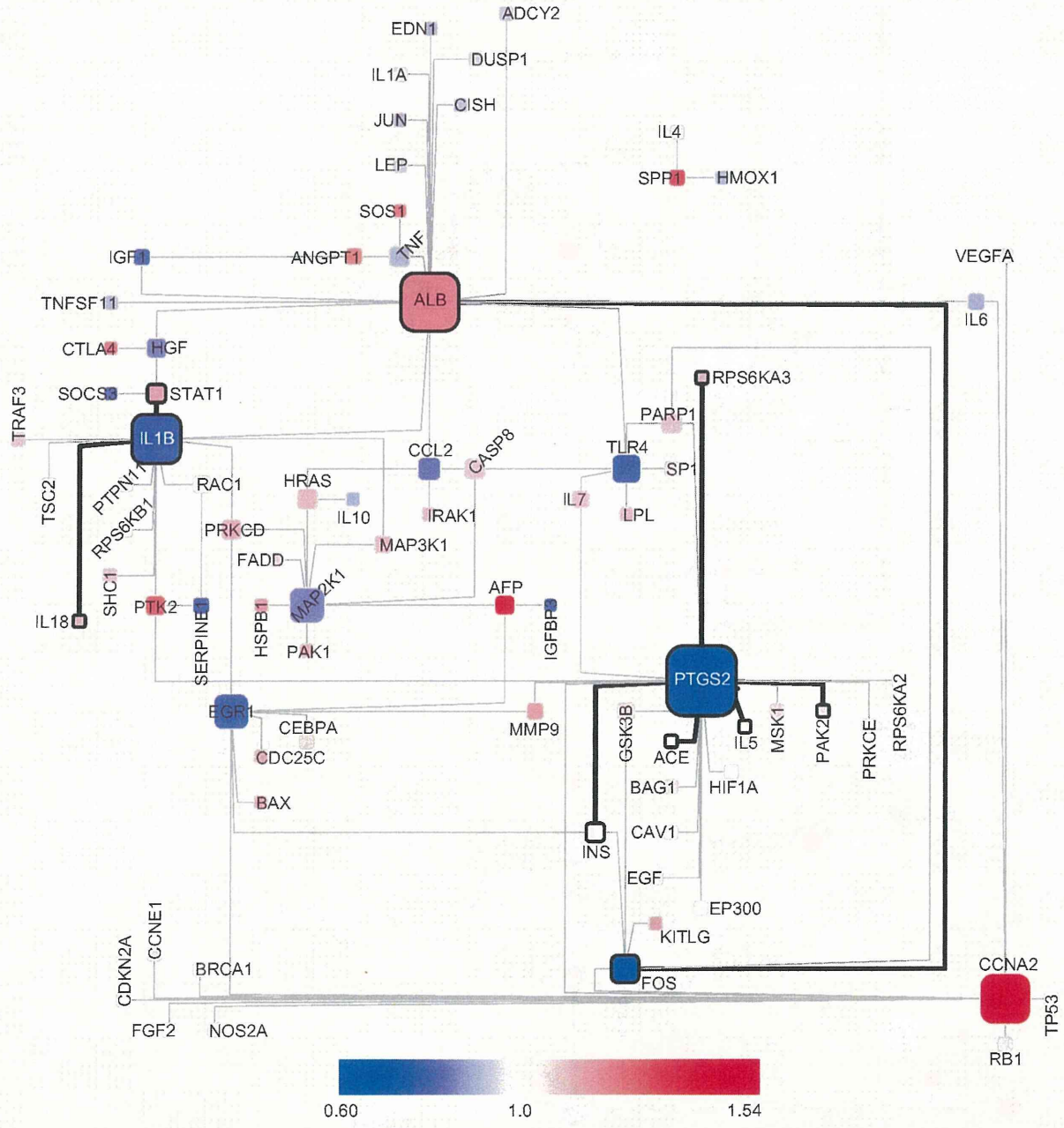

Figure 7. Changes in ON/OFF states of BTSs in dysplastic liver tissue and hepatocellular carcinoma. BTS toggling graph comparing the mRNA expression data (ArrayExpress ID: E-GEOD-6764) of normal liver tissue with that of precancerous and cancerous liver tissue. The nodes and edges surrounded by the bold lines are BTSs for which toggling was observed when comparing dysplastic liver tissue, a precursor of liver cancer, with normal liver tissue. The nodes represent genes and the edges between them represent the pairing of bistable toggle switches. The colors of nodes were automatically assigned as a continuous color gradient from red for ON (upregulated) to blue for OFF (downregulated) according to relative gene-expression levels of the nodes.
doi:10.1371/journal.pcbi.1000851.g007

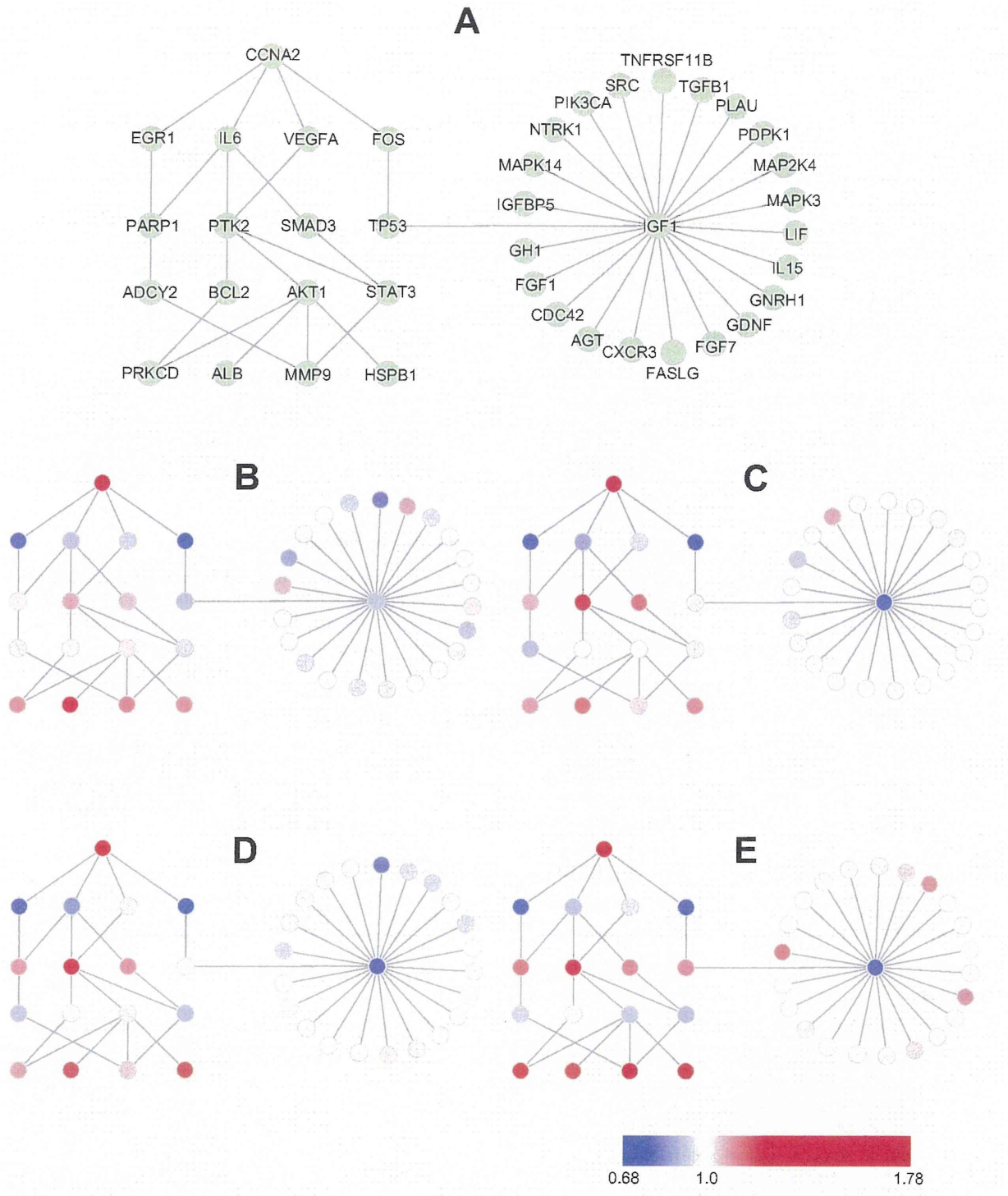

Figure 8. Rippling of toggling of CCNA2-related BTS during malignant transition of HCC. Fig. 8A: A network of CCNA2-related BTS pairs selected from the data used in Fig. 7A. Fig. 8B–E: The nodes represent genes and the edges between them represent the pairing of bistable toggle switches. The colors of nodes were automatically assigned as a continuous color gradient from red for ON (upregulated) to blue for OFF (downregulated) according to relative gene-expression levels of the nodes. B: very early HCC, C: early HCC, D: advanced HCC, E: very advanced HCC. Note that the ON/OFF status of TP53-IGF1 was changed in advanced HCC.
doi:10.1371/journal.pcbi.1000851.g008

expression regulation, direct regulation, molecular transport regulation, and molecular synthesis regulation). MedScan also extracted information on the relation direction and the effect on the target molecule. The "Effect" attribute has three possible values: "positive," "negative," and "unknown." The BTS pairs were extracted from the database on the basis of five rules.

(1) Nodes are limited to genes and proteins only.
(2) Edges are limited to "Regulation," "Expression," and "DirectRegulation."
(3) "Unknown" edges in the "Effect" attribute are omitted.
(4) Edges extracted from fewer than three references are omitted.
(5) If there is a positive and negative attribute in the same direction, the edge is extracted from additional references.

We extracted 19,178 relationships involving 3,682 genes (basic interaction datasets).

Extraction of candidate bistable toggle switches

Using basic interaction datasets, we extracted possible network motifs for toggle switches. We defined these motifs as follows.

The type-1 BTS contains two genes that have positive autoregulation and inhibit each other's expression. The type-2 BTS also contains two genes that suppress each other's expression, but each gene also has a positive or negative loop with the other gene. One of the four subtypes of type-2 BTSs (corresponding to the four possible combinations of double positive and/or negative feedback) shows the same function as the type-1 BTS. The type-3 BTS was based on a theoretical study of the modeling of genetic switches with positive feedback loops [37]. The BTS motifs are illustrated in Fig. 2, and we extracted 6585 BTSs (see supporting Table 1).

Analysis of toggling

We used mRNA microarray data to examine the changes in the ON/OFF states of BTS candidates. CEL format files or tab-limited text files were downloaded via ArrayExpress (http://www.ebi.ac.uk/arrayexpress/), which is a public repository provided by the European Bioinformatics Institute [68]. We only used microarray data obtained from experiments with humans and with platforms of Affymetrix HG-U133A&B (631 sets) and HG-U133Plus2.0 (404 sets). These data were normalized and summarized using the robust multichip analysis method [69] implemented in the Affymetrix Expression Console software.

The toggling of a BTS pair was defined as instances in which the mRNA levels of a sample increased for one molecule of the pair and decreased for the other. To remove background noise, we calculated the toggling score using

$$\text{toggling score} = (\text{SW1 sample value}/\text{SW1 control value}) / (\text{SW2 sample value}/\text{SW2 control value}),$$

where SW1 and SW2 are the two molecules in alphabetical order. Changes in the ON/OFF states were considered significant when the toggling score was more than two standard deviations greater than the mean of all the toggling scores.

Network visualization

For pathway visualization, we used Cytoscape (Version 2.6.3), which is widely used open-source software for visualization and analysis of networks [70]. The nodes in the visualized BTS network represent genes, the edges between nodes represent the pairing of bistable toggle switches, and the color of nodes were automatically assigned as a continuous color gradient from red for ON (upregulated) to blue for OFF (downregulated) according to relative gene-expression levels of the nodes.

Supporting Information

Protocol S1 List of BTS pairs SW1 and SW2 are the two molecules comprising a BTS pair in alphabetical order.
Found at: doi:10.1371/journal.pcbi.1000851.s001 (0.16 MB XLS)

Protocol S2 Cytoscape session file for Figure 3.
Found at: doi:10.1371/journal.pcbi.1000851.s002 (0.09 MB ZIP)

Acknowledgments

We are grateful to Dr. Y. Hamada (Sony Corporation) for preparing the basic interaction datasets, Mr. J. Suzuki (Tokyo Institute of Technology) for assisting us with the data extraction, and Dr. S. Ueda (Otsu Municipal Hospital) for providing us with the microarray data. We also thank Dr. K. Tabuchi for his useful comments and discussion.

Author Contributions

Conceived and designed the experiments: TS SM HK. Performed the experiments: TS. Analyzed the data: TS SM. Contributed reagents/materials/analysis tools: TS SM. Wrote the paper: TS HK.

References

1. Sontag ED (2007) Monotone and near-monotone biochemical networks. Syst Synth Biol 1: 59–87.
2. Kauffman S, Peterson C, Samuelsson B, Troein C (2004) Genetic networks with canalyzing Boolean rules are always stable. Proc Natl Acad Sci USA 101: 17102–17107.
3. Milo R, Shen-Orr S, Itzkovitz S, Kashtan N, Chklovskii D, et al. (2002) Network motifs: simple building blocks of complex networks. Science 298: 824–827.
4. Shen-Orr SS, Milo R, Mangan S, Alon U (2002) Network motifs in the transcriptional regulation network of Escherichia coli. Nat Genet 31: 64–68.
5. Tyson JJ, Chen KC, Novak B (2003) Sniffers, buzzers, toggles and blinkers: dynamics of regulatory and signaling pathways in the cell. Curr Opin Cell Biol 15: 221–231.
6. Wolf DM, Arkin AP (2003) Motifs, modules and games in bacteria. Curr Opin Microbiol 6: 125–134.
7. Isaacs FJ, Hasty J, Cantor CR, Collins JJ (2003) Prediction and measurement of an autoregulatory genetic module. Proc Natl Acad Sci USA 100: 7714–7719.
8. McAdams HH, Arkin A (1997) Stochastic mechanisms in gene expression. Proc Natl Acad Sci USA 94: 814–819.
9. Ptashne M (1992) A genetic switch; phage lambda and higher organisms. Blackwell Science.
10. Novick A, Weiner M (1957) Enzyme Induction as an all-or-none phenomenon. Proc Natl Acad Sci USA 43: 553–566.
11. Ozbudak EM, Thattai M, Lim HN, Shraiman BI, Van Oudenaarden A (2004) Multistability in the lactose utilization network of Escherichia coli. Nature 427: 737–740.
12. Vilar JM, Guet CC, Leibler S (2003) Modeling network dynamics: the lac operon, a case study. J Cell Biol 161: 471–476.
13. Bagowski CP, Ferrell JE, Jr. (2001) Bistability in the JNK cascade. Curr Biol 11: 1176–1182.
14. Bhalla US, Ram PT, Iyengar R (2002) MAP kinase phosphatase as a locus of flexibility in a mitogen-activated protein kinase signaling network. Science 297: 1018–1023.
15. Ferrell JE, Jr. (1996) Tripping the switch fantastic: how a protein kinase cascade can convert graded inputs into switch-like outputs. Trends Biochem Sci 21: 460–466.
16. Ferrell JE, Jr. (1997) How responses get more switch-like as you move down a protein kinase cascade. Trends Biochem Sci 22: 288–289.
17. Ferrell JE, Jr., Machleder EM (1998) The biochemical basis of an all-or-none cell fate switch in Xenopus oocytes. Science 280: 895–898.
18. Ferrell JE, Xiong W (2001) Bistability in cell signaling: How to make continuous processes discontinuous, and reversible processes irreversible. Chaos 11: 227–236.

19. Huang CY, Ferrell JE, Jr. (1996) Ultrasensitivity in the mitogen-activated protein kinase cascade. Proc Natl Acad Sci USA 93: 10078–10083.
20. Markevich NI, Hoek JB, Kholodenko BN (2004) Signaling switches and bistability arising from multisite phosphorylation in protein kinase cascades. J Cell Biol 164: 353–359.
21. Lai K, Robertson MJ, Schaffer DV (2004) The sonic hedgehog signaling system as a bistable genetic switch. Biophys J 86: 2748–2757.
22. Cross FR, Archambault V, Miller M, Klovstad M (2002) Testing a mathematical model of the yeast cell cycle. Mol Biol Cell 13: 52–70.
23. Pomerening JR, Sontag ED, Ferrell JE, Jr. (2003) Building a cell cycle oscillator: hysteresis and bistability in the activation of Cdc2. Nat Cell Biol 5: 346–351.
24. Sha W, Moore J, Chen K, Lassaletta AD, Yi CS, et al. (2003) Hysteresis drives cell-cycle transitions in Xenopus laevis egg extracts. Proc Natl Acad Sci USA 100: 975–980.
25. Reynolds AR, Tischer C, Verveer PJ, Rocks O, Bastiaens PI (2003) EGFR activation coupled to inhibition of tyrosine phosphatases causes lateral signal propagation. Nat Cell Biol 5: 447–453.
26. Gardner TS, Cantor CR, Collins JJ (2000) Construction of a genetic toggle switch in Escherichia coli. Nature 403: 339–342.
27. Kobayashi H, Kaern M, Araki M, Chung K, Gardner TS, et al. (2004) Programmable cells: interfacing natural and engineered gene networks. Proc Natl Acad Sci USA 101: 8414–8419.
28. Kramer BP, Viretta AU, Daoud-El-Baba M, Aubel D, Weber W, et al. (2004) An engineered epigenetic transgene switch in mammalian cells. Nat Biotechnol 22: 867–870.
29. Sabouri-Ghomi M, Ciliberto A, Kar S, Novak B, Tyson JJ (2008) Antagonism and bistability in protein interaction networks. J Theor Biol 250: 209–218.
30. Bagowski CP, Besser J, Frey CR, Ferrell JE, Jr. (2003) The JNK cascade as a biochemical switch in mammalian cells: ultrasensitive and all-or-none responses. Curr Biol 13: 315–320.
31. Laslo P, Spooner CJ, Warmflash A, Lancki DW, Lee HJ, et al. (2006) Multilineage transcriptional priming and determination of alternate hematopoietic cell fates. Cell 126: 755–766.
32. Ferrell JE, Jr. (2002) Self-perpetuating states in signal transduction: positive feedback, double-negative feedback and bistability. Curr Opin Cell Biol 14: 140–148.
33. Hasty J, McMillen D, Isaacs F, Collins JJ (2001) Computational studies of gene regulatory networks: in numero molecular biology. Nat Rev Genet 2: 268–279.
34. Laurent M, Kellershohn N (1999) Multistability: a major means of differentiation and evolution in biological systems. Trends Biochem Sci 24: 418–422.
35. Smolen P, Baxter DA, Byrne JH (2000) Mathematical modeling of gene networks. Neuron 26: 567–580.
36. Guantes R, Poyatos JF (2008) Multistable decision switches for flexible control of epigenetic differentiation. PLoS Comput Biol 4: e1000235.
37. Kobayashi T, Chen L, Aihara K (2003) Modeling genetic switches with positive feedback loops. J Theor Biol 221: 379–399.
38. Cao Y, Liang J (2008) Optimal enumeration of state space of finitely buffered stochastic molecular networks and exact computation of steady state landscape probability. BMC Syst Biol 2: 30.
39. Chatterjee A, Kaznessis YN, Hu WS (2008) Tweaking biological switches through a better understanding of bistability behavior. Curr Opin Biotechnol 19: 475–481.
40. Okita K, Nakagawa M, Hyenjong H, Ichisaka T, Yamanaka S (2008) Generation of mouse induced pluripotent stem cells without viral vectors. Science 322: 949–953.
41. Boyer LA, Mathur D, Jaenisch R (2006) Molecular control of pluripotency. Curr Opin Genet Dev 16: 455–462.
42. Chickarmane V, Troein C, Nuber UA, Sauro HM, Peterson C (2006) Transcriptional dynamics of the embryonic stem cell switch. PLoS Comput Biol 2: e123.
43. Niwa H (2007) How is pluripotency determined and maintained? Development 134: 635–646.
44. Chari R, Lonergan KM, Ng RT, MacAulay C, Lam WL, et al. (2007) Effect of active smoking on the human bronchial epithelium transcriptome. BMC Genomics 8: 297.
45. Sridhar S, Schembri F, Zeskind J, Shah V, Gustafson AM, et al. (2008) Smoking-induced gene expression changes in the bronchial airway are reflected in nasal and buccal epithelium. BMC Genomics 9: 259.
46. Gao H, Ward PA (2007) STAT3 and suppressor of cytokine signaling 3: potential targets in lung inflammatory responses. Expert Opin Ther Targets 11: 869–880.
47. He B, You L, Uematsu K, Zang K, Xu Z, et al. (2003) SOCS-3 is frequently silenced by hypermethylation and suppresses cell growth in human lung cancer. Proc Natl Acad Sci USA 100: 14133–14138.
48. Boldrini L, Donati V, Dell'Omodarme M, Prati MC, Faviana P, et al. (2005) Prognostic significance of osteopontin expression in early-stage non-small-cell lung cancer. Br J Cancer 93: 453–457.
49. Boldrini L, Gisfredi S, Ursino S, Faviana P, Lucchi M, et al. (2005) Expression of endothelin-1 is related to poor prognosis in non-small cell lung carcinoma. Eur J Cancer 41: 2828–2835.
50. Davis GL, Dempster J, Meler JD, Orr DW, Walberg MW, et al. (2008) Hepatocellular carcinoma: management of an increasingly common problem. Proc (Bayl Univ Med Cent) 21: 266–280.
51. Wurmbach E, Chen YB, Khitrov G, Zhang W, Roayaie S, et al. (2007) Genome-wide molecular profiles of HCV-induced dysplasia and hepatocellular carcinoma. Hepatology 45: 938–947.
52. Bae SH, Jung ES, Park YM, Kim BS, Kim BK, et al. (2001) Expression of cyclooxygenase-2 (COX-2) in hepatocellular carcinoma and growth inhibition of hepatoma cell lines by a COX-2 inhibitor, NS-398. Clin Cancer Res 7: 1410–1418.
53. Baek JY, Hur W, Wang JS, Bae SH, Yoon SK (2007) Selective COX-2 inhibitor, NS-398, suppresses cellular proliferation in human hepatocellular carcinoma cell lines via cell cycle arrest. World J Gastroenterol 13: 1175–1181.
54. Wheeler LW, Lents NH, Baldassare JJ (2008) Cyclin A-CDK activity during G1 phase impairs MCM chromatin loading and inhibits DNA synthesis in mammalian cells. Cell Cycle 7: 2179–2188.
55. Krones-Herzig A, Mittal S, Yule K, Liang H, English C, et al. (2005) Early growth response 1 acts as a tumor suppressor in vivo and in vitro via regulation of p53. Cancer Res 65: 5133–5143.
56. Hao MW, Liang YR, Liu YF, Liu L, Wu MY, et al. (2002) Transcription factor EGR-1 inhibits growth of hepatocellular carcinoma and esophageal carcinoma cell lines. World J Gastroenterol 8: 203–207.
57. Elsammak MY, Amin GM, Khalil GM, Ragab WS, Abaza MM (2006) Possible contribution of serum activin A and IGF-1 in the development of hepatocellular carcinoma in Egyptian patients suffering from combined hepatitis C virus infection and hepatic schistosomiasis. Clin Biochem 39: 623–629.
58. Qiao L, Nachbar RB, Kevrekidis IG, Shvartsman SY (2007) Bistability and oscillations in the Huang-Ferrell model of MAPK signaling. PLoS Comput Biol 3: 1819–1826.
59. Niwa H, Toyooka Y, Shimosato D, Strumpf D, Takahashi K (2005) Interaction between Oct3/4 and Cdx2 determines trophectoderm differentiation. Cell 123: 917–929.
60. Wang ES, Szabo SJ, Schwartberg PL, Glimcher LH (2005) T helper cell fate specified by kinase-mediated interaction of T-bet with GATA-3. Science 307: 430–433.
61. Schwarz M, Cecconi F, Bernier G, Andrejewski N, Kammandel B, et al. (2000) Spatial specification of mammalian eye territories by reciprocal transcriptional repression of Pax2 and Pax6. Development 127: 4325–4334.
62. Asyali MH, Shoukri MM, Demirkaya O, Khabar KS (2004) Assessment of reliability of microarray data and estimation of signal thresholds using mixture modeling. Nucleic Acids Res 32: 2323–2335.
63. Hinkley DV (1969) On the ratio of two correlated normal random variables. Biometrika 56: 635–639.
64. Brody JP, Williams BA, Wold BJ, Quake SR (2002) Significance and statistical errors in the analysis of DNA microarray data. Proc Natl Acad Sci USA 99: 12975–12978.
65. Cochella L, Green R (2005) Fidelity in protein synthesis. Curr Biol 15: R536–540.
66. Xu Y, Chen SY, Ross KN, Balk SP (2006) Androgens induce prostate cancer cell proliferation through mammalian target of rapamycin activation and post-transcriptional increases in cyclin D proteins. Cancer Res 66: 7783–7792.
67. Novichkova S, Egorov S, Daraselia N (2003) MedScan, a natural language processing engine for MEDLINE abstracts. Bioinformatics 19: 1699–1706.
68. Parkinson H, Kapushesky M, Shojatalab M, Abeygunawardena N, Coulson R, et al. (2007) ArrayExpress—a public database of microarray experiments and gene expression profiles. Nucleic Acids Res 35: D747–750.
69. Irizarry RA, Hobbs B, Collin F, Beazer-Barclay YD, Antonellis KJ, et al. (2003) Exploration, normalization, and summaries of high density oligonucleotide array probe level data. Biostatistics 4: 249–264.
70. Shannon P, Markiel A, Ozier O, Baliga NS, Wang JT, et al. (2003) : Cytoscape: a software environment for integrated models of biomolecular interaction networks. Genome Res 13: 2498–2504.

BIOINFORMATICS APPLICATIONS NOTE Vol. 26 no. 10 2010, pages 1381–1383
doi:10.1093/bioinformatics/btq143

Systems biology

Advance Access publication April 5, 2010

Payao: a community platform for SBML pathway model curation

Yukiko Matsuoka[1,2], Samik Ghosh[1], Norihiro Kikuchi[3] and Hiroaki Kitano[1,4,5,*]

[1]The Systems Biology Institute, Tokyo, [2]JST ERATO Kawaoka Infection-induced Host-response Network Project, Tokyo, [3]Mitsui Knowledge Industry Co. Ltd, Tokyo, [4]Okinawa Institute of Science and Technology, Okinawa and [5]Sony Computer Science Laboratories, Tokyo, Japan

Associate Editor: Jonathan Wren

ABSTRACT

Summary: Payao is a community-based, collaborative web service platform for gene-regulatory and biochemical pathway model curation. The system combines Web 2.0 technologies and online model visualization functions to enable a collaborative community to annotate and curate biological models. Payao reads the models in Systems Biology Markup Language format, displays them with CellDesigner, a process diagram editor, which complies with the Systems Biology Graphical Notation, and provides an interface for model enrichment (adding tags and comments to the models) for the access-controlled community members.

Availability and implementation: Freely available for model curation service at http://www.payaologue.org. Web site implemented in Seaser Framework 2.0 with S2Flex2, MySQL 5.0 and Tomcat 5.5, with all major browsers supported.

Contact: kitano@sbi.jp

Received on January 21, 2010; revised on March 12, 2010; accepted on March 30, 2010

1 INTRODUCTION

Creating an extensive model of gene-regulatory and biochemical networks with the latest data is a painstaking task. Curation is essential to creating an accurate model. Yet as science and technology advances rapidly, once curated models soon become out-of-date and need to be revised constantly. Many pathways and networks are now available online via pathway databases, such as Reactome, BioModels.net, Panther Pathways and many pathway editors are available (Bauer-Mehren *et al.*, 2009). What is needed is a framework to facilitate tracking and update mechanism for modelers and researchers in the community to contribute to the collaborative model building and curation process.

WikiPathways (Pico *et al.*, 2008) is an effort for such a collaborative platform in the Wiki style. While the Wiki system has its strength in collaborative editing and version tracking, it does not provide access control or explicit community tagging mechanisms. In a community-driven model enrichment environment, it is effective to differentiate privileges to special interest group (SIG) members for curation activities—commenting on existing tags, adding tags to models, annotating individual component inside a model and validating the annotations. In view of the complexity of biological pathways and the expertise of biologists in different areas, a community platform for biology requires an exquisite balance of federated resource sharing and quality control of information by a SIG of experts in the particular pathway or process. An access control privilege system allows the community to share and disseminate the knowledge, while enabling a dedicated SIG to maintain high-quality, curated information.

To provide such a curation framework, we have developed a system called 'Payao'. The system is named after a fish aggregating device, an artificial floating raft where fish congregate and popular in Okinawa/Philippine area. Payao aims to become a biological knowledge aggregating system, which enable a community to work on the same models simultaneously, insert tags as pop-up balloon to the parts of the model, exchange comments, record the discussions and eventually update the models accurately and concurrently.

The current workflow for pathway curation has two phases working in a cyclical manner, as shown in Figure 1: pathway editing using biological pathway editors (CellDesigner) and community-driven pathway enrichment and knowledge sharing. Payao serves for enrichment phase of the curation. Payao is a web-based platform, providing an interface for adding tags and comments to the components (such as Species, Reactions and specified area) of the model, as well as community management functionality. The information on the users and tag data is stored in a relational database (RDBMS) on the server. Payao adopts community standards, accepting Systems Biology Markup Language (SBML; Hucka *et al.*, 2003) format models and displays them in Systems Biology Graphical Notation (Le Novere *et al.*, 2009) compliant CellDesigner (Funahashi *et al.*, 2008) graphical notation. Curation data on Payao can be easily reintegrated into the original model via CellDesigner.

Fig. 1. Workflow of community pathway curation.

*To whom correspondence should be addressed.

2 PLATFORM

Payao consists of the server application, client user interface and database. The server application has been implemented in Java on Seaser Framework 2.0 with S2Flex2. Tomcat 5.5 was used as the servlet container to build the web application. The client user interface has been implemented in ActionScript on Flex framework 2.0.1, which allows us to build a Rich Internet Application to visualize SBML models. The server communicates with the client via the Action Message Format (AMF3) protocol on S2Flex2, which enables us to translate between Java Objects in Seaser and Action Script Object in Flex. The server can handle CellDesigner models including SBML models and the visual information using CellDesigner API ver.4.0. It parses SBML files sent from client to create CellDesigner models, and provides the information as CellDesigner Plugin classes. The client application receives the model information and draws the model. MySQL 5.0 is used to store information on user, model and tags/comments in the database.

3 FEATURES

As Payao accepts pathway models stored in SBML format and uses CellDesigner APIs for visualization, the most suitable SBML editor for Payao is CellDesigner. In SBML format, models can capture details of biochemical process descriptions, not only protein–protein interactions. Adopting SBML format enables the models to be easily used as the base of computational data analysis or simulation of dynamic behaviors. The Payao platform enriches the model curation process by providing a host of features for user management, tagging and model updates [detailed are available for reference in (Payao User guide, 2009)].

3.1 Community management

Forming a community is an important step for curation. Different expertise groups can contribute variety of information to the model. As web-based Payao can be accessible from all physical locations, it enables experts across the world to communicate in a collaborative curation effort.

Community is formed around a pathway model. It is the model owner who sets access control over the registered model. In the Payao system, access controls can be set by specifying the privileges to individuals as well as to user categories, such as guest, login user and model user (who are invited to access the model by the model owner). This enables a user to stage the curation process, initiate the curation within a small group (e.g. SIG) and then switch the access control of the model for public viewing.

3.2 Model management

The model owner registers and manages the SBML model. Upon registration, the model owner specifies the basic model information including, thumbnail image, references and copyright. The owner sets the access privilege to the user in three levels (browsing, adding tags, adding comments) by user categories or by individual users. The registered models can be sorted by Register Date and by Popularity. Popularity is measured by the activity level (number of tags and comments) and ranked in the list. All the registered models are listed with the thumbnails in the top screen in the right panel (Fig. 2). Registered models are stored in the database.

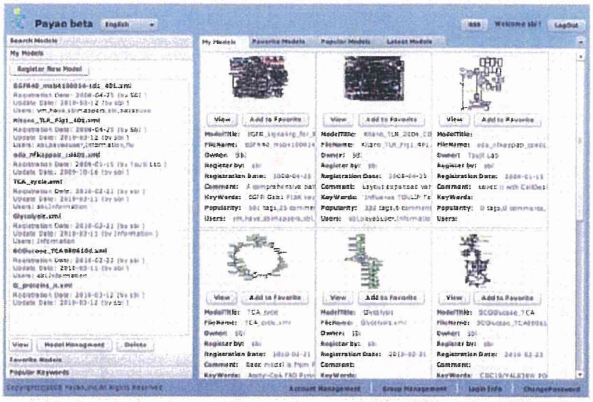

Fig. 2. Payao Model Browser screen—browse the registered models in the list format (left) and the thumbnails with summary data and statistics (right).

3.3 Community tagging and commenting

The tagging on the visually represented pathways is a characteristic of Payao, which makes the curators easy to grasp the nature of the pathway while discussing on the specific component of the pathways. Like Google Maps, tags are displayed in a bubble form attached to the items (Species, Reactions or any specified area), and click to expand and display the content of the information in the tag. Tags can specifically be keywords, links, PubMed IDs as well as free text, as shown in Figure 3. A TagSet groups a set of tags and can be color coded for ease of viewing. User-defined TagSets also allow access control features (browsing, editing and editing tags) to be set by a user, in the same way as for model access privilege settings. Thus, a user can set permissions to a 'My Tagset', which hides comments and tags from the community members. Inside the tag, comments can be added in the free text format. While tags anchor the points for annotation in the model, comments function serves as the discussion space.

3.4 Model update: tag data export and import

Data in the tags can be exported from the Payao system, evaluated outside the system and integrated into the Payao system or to the SBML model file. All the information, including the model file (CellDesigner format), Tags/Comments and model image (png/jpg/pdf format) in a ZIP file format are exported in a batch. Information stored in Tags is exported as a table in .csv format, which can be edited and imported back to the system. The tag information can also be imported into the base CellDesigner-format model as 'notes' using a CellDesigner plugin (import notes) and stored in SBML 'notes' annotation. Once the base model has been updated using CellDesigner, the model owner can reregister the model onto Payao for further curation.

4 FUTURE DEVELOPMENT

Payao will facilitate the evolution of CellDesigner from a simple tag-based pathway curation tool to a more versatile, comprehensive platform. The next version of CellDesigner will adopt support for Minimum Information Required in the Annotation of Models (MIRIAMs; Le Novère *et al.*, 2005) standard for annotation and

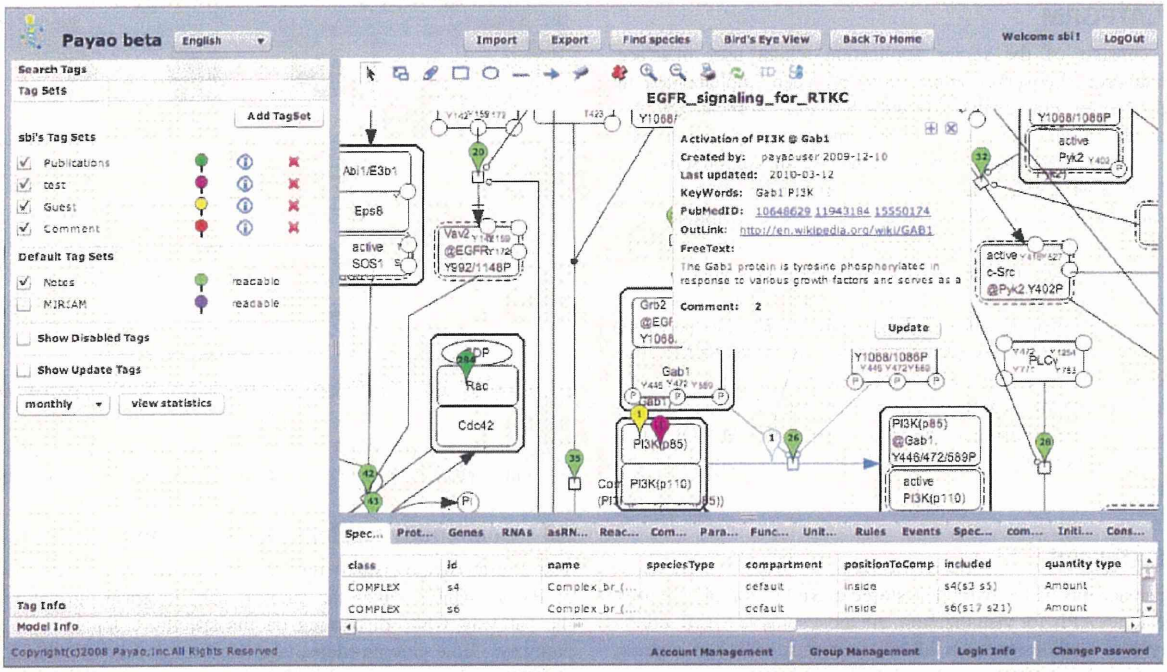

Fig. 3. Payao Model Viewer screenshot—model view panel and tag example. In the left panel, tagsets are listed to identify by specified color. In the right panel, under the tagset, assigned model users can add/edit tags associated with the nodes/reactions. Other users can add comments to the tag for providing further information or raising an issue against the tag contents.

allow MIRIAM annotations to be viewed on Payao. Modules to support import of different pathway exchange formats (BioPax), visual mapping of experimental data on pathway components in Payao, would be developed in future versions. Future enhancements also include integration of Payao with biological text mining techniques to facilitate literature-driven knowledge enrichment of existing pathway models. Tracking model updates using an RSS (Really Simple Syndication) feed will assist curators as well as public viewers. Statistics for measuring contribution of individuals to the model curation process as well as community interest (measured by count of tags and comments on a model) would be integrated into Payao in future releases. In the long run, we envisage this system to be a platform for aggregation, dissemination and community exchange for biological pathway models.

Funding: Okinawa Institute of Science and Technology (http://www.oist.jp); Establishment of a Human Genome Network Project (MEXT); Japan Science and Technology Agency/Biotechnology and Biological Sciences Research Council Strategic International Corporation Program; The Systems Biology Institute.

Conflict of Interest: none declared.

REFERENCES

Bauer-Mehren,A. *et al.* (2009) Pathway databases and tools for their exploitation: benefits, current limitations and challenges. *Mol. Syst. Biol.*, **5**, 290.

Funahashi,A. *et al.* (2008) CellDesigner 3.5: a versatile modeling tool for biochemical networks. *Pro. IEEE*, **96**, 1254–1265.

Hucka,M. *et al.* (2003) The systems biology markup language (SBML): a medium for representation and exchange of biochemical network models. *Bioinformatics*, **19**, 524–531.

Le Novère,N. *et al.* (2005) Minimum information requested in the annotation of biochemical models (MIRIAM). *Nat. Biotechnol.*, **23**, 1509–1515.

Le Novère, N. *et al.* (2009) Systems biology graphical notation. *Nat. Biotech.*, **8**, 735–741.

Pico,A. *et al.* (2008) WikiPathways: pathway editing for the people. *PLoS Biol.*, **6**, e184.

Payao User Guide. (2009) Available at http://celldesigner.org/payao/payaopreview.html (last accessed date April 1, 2010)

MOLECULAR AND CELLULAR BIOLOGY, Dec. 2009, p. 6391–6400 Vol. 29, No. 24
0270-7306/09/$12.00 doi:10.1128/MCB.00337-09

Hypersensitivity of Aryl Hydrocarbon Receptor-Deficient Mice to Lipopolysaccharide-Induced Septic Shock▽†

Hiroki Sekine,[1,5] Junsei Mimura,[1,5] Motohiko Oshima,[1,5] Hiromi Okawa,[1,5] Jun Kanno,[2] Katsuhide Igarashi,[2] Frank J. Gonzalez,[3] Togo Ikuta,[4] Kaname Kawajiri,[4] and Yoshiaki Fujii-Kuriyama[1,5]*

The Center for Tsukuba Advanced Research Alliance and Institute of Basic Medical Sciences, University of Tsukuba, 1-1-1 Tennoudai, Tsukuba 305-8577, Japan[1]; Division of Molecular Toxicology, National Institute of Health Sciences, 1-18-1 Kamiyoga, Setagaya-ku, Tokyo 158-8501, Japan[2]; Laboratory of Metabolism, Center for Cancer Research, National Cancer Institute, National Institutes of Health, Bethesda, Maryland 20892[3]; Research Institute for Clinical Oncology, Saitama Cancer Center, 818 Komuro, Ina-machi, Kitaadachi-gun, Saitama 362-0806, Japan[4]; and SORST, Japan Science and Technology Agency, 4-1-8 Honcho, Kawaguchi, 332-0012, Japan[5]

Received 16 March 2009/Returned for modification 2 May 2009/Accepted 11 September 2009

Aryl hydrocarbon receptor (AhR), a ligand-activated transcription factor, is known to mediate a wide variety of pharmacological and toxicological effects caused by polycyclic aromatic hydrocarbons. Recent studies have revealed that AhR is involved in the normal development and homeostasis of many organs. Here, we demonstrate that AhR knockout (AhR KO) mice are hypersensitive to lipopolysaccharide (LPS)-induced septic shock, mainly due to the dysfunction of their macrophages. In response to LPS, bone marrow-derived macrophages (BMDM) of AhR KO mice secreted an enhanced amount of interleukin-1β (IL-1β). Since the enhanced IL-1β secretion was suppressed by supplementing Plasminogen activator inhibitor-2 (Pai-2) expression through transduction with Pai-2-expressing adenoviruses, reduced Pai-2 expression could be a cause of the increased IL-1β secretion by AhR KO mouse BMDM. Analysis of gene expression revealed that AhR directly regulates the expression of Pai-2 through a mechanism involving NF-κB but not AhR nuclear translocator (Arnt), in an LPS-dependent manner. Together with the result that administration of the AhR ligand 3-methylcholanthrene partially protected mice with wild-type AhR from endotoxin-induced death, these results raise the possibility that an appropriate AhR ligand may be useful for treating patients with inflammatory disorders.

The aryl hydrocarbon receptor (AhR) is a member of the basic helix-loop-helix/Per-Arnt-Sim homology superfamily and is involved in the induction of drug-metabolizing enzymes and the susceptibility of cells to a variety of cytotoxicities induced by dioxins (9). AhR is a ligand-activated transcription factor activated by polycyclic aromatic hydrocarbons (PAHs), such as 3-methylcholanthrene (3MC) and 2′,3′,7′,8′-tetrachlorodibenzo-*p*-dioxin (TCDD). Under normal conditions, AhR exists in the cytoplasm in a complex with Hsp90, XAP2, and p23 (22). After binding a ligand, AhR translocates into the nucleus where it dimerizes with its partner molecule, AhR nuclear translocator (Arnt), and acts as a transcriptional activator to regulate the expression of target genes, such as those expressing drug-metabolizing cytochrome P450 (Cyp1a1, 1a2, and 1b1) and NAD(P)H: quinone oxidoreductase (Nqo), by binding to xenobiotic response element (XRE) sequences in their promoter regions (9). By using AhR knockout (AhR KO) mice, it has been demonstrated that AhR is essential not only for the induction of drug-metabolizing enzymes but also for most, if not all, of the toxicological effects caused by TCDD, including immunosuppression, thymic atrophy, teratogenesis, and hyperplasia (6, 7, 17, 24), the mechanisms for which are largely unknown. Recently, careful investigation into the loss of functions in AhR KO mice has also revealed that AhR is involved in the normal development of several organs, including the liver, heart, vascular tissues, and reproductive organs (1, 2, 6, 8, 15, 24). In addition, AhR has been found to play a key role in the differentiation of regulatory T cells Treg, Th17, and Th1 from naive CD4 T cells by regulating their expression of Foxp3 or by as-yet-unknown mechanisms (14, 20, 23, 32). From these studies, one of the general features of AhR that begins to emerge is that it serves as a multifunctional regulator in a large number of areas, ranging from drug metabolism to innate immunity for protection against invasive xenobiotics. In the work presented here, we demonstrated that AhR KO mice were hypersensitive to lipopolysaccharide (LPS)-induced septic shock, mainly due to the dysfunction of their macrophages. AhR KO mouse macrophages secreted an enhanced amount of interleukin-1β (IL-1β) in response to LPS treatment and had markedly reduced Plasminogen activator inhibitor-2 (Pai-2) mRNA concentrations, as revealed by DNA microarray analysis. Pai-2 was reported to be a negative regulator of IL-1β secretion through its inhibition of caspase-1 (10), suggesting that the enhanced secretion of IL-1β by AhR KO macrophages in response to LPS may have been due to the reduced level of Pai-2. We showed that AhR directly regulates the expression of inhibitory Pai-2, in an LPS-dependent manner, through a mechanism involving NF-κB but not Arnt.

* Corresponding author. Present address: 5-18-7 Honkomagome, Bunkyo-ku, Tokyo 113-0021, Japan. Phone and fax: 3-3941-2200. E-mail: y.k_fujii@nifty.com.

† Supplemental material for this article may be found at http://mcb.asm.org/.

▽ Published ahead of print on 12 October 2009.

MATERIALS AND METHODS

Mice. AhR knockout (AhR KO) mice were generated as described previously (17). These mice were back-crossed with C57BL/6J mice at least 10 times. Age-matched mice (10 weeks) were intraperitoneally injected with 20 mg of

LPS/kg of body weight. Mice with floxed *Arnt* (30) and *AhR* (Jackson laboratory) alleles were crossed to LysM Cre mice to specifically delete these genes in their macrophages. $AhR^{flox/-}$ and $AhR^{flox/-}$::LysM Cre mice were generated by mating $AhR^{flox/flox}$::LysM Cre and $AhR^{-/-}$ (AhR KO) mice. These age-matched mice (9 to 11 weeks old) were intraperitoneally injected with 25 mg LPS/kg. Mouse survival was checked every 6 or 12 h. 3MC (Wako, Osaka) at 10 μl (4 mg/ml 3MC)/g of body weight or 10 μl corn oil/g was intraperitoneally injected. After 2 h, each mouse was intraperitoneally injected with 30 mg LPS/kg. LPS (from *Escherichia coli* 0111:B4) was purchased from Sigma.

Preparation of macrophages. Bone marrow cells were obtained from the femurs of 8- to 12-week-old mice. The bone marrow-derived macrophages (BMDM) used for each experiment were isolated by culturing bone marrow cells in the presence of 10 ng/ml granulocyte-macrophage colony-stimulating factor (PeproTech) for 7 days and washing the attached cells with phosphate-buffered saline (PBS) three times. For cytokine assays, washed cells were collected with a scraper, plated at 2×10^6 cells/ml in 96-well plates, and cultured with 10 ng/ml LPS for 8 h.

For isolation of peritoneal exudate macrophages (PEMs), mice were intraperitoneally injected with 2 ml of 4% thioglycolate. Peritoneal cells were isolated from exudates of the peritoneal cavity 3 days after injection, incubated for 3 h in appropriate plates, and washed with PBS. The adherent cells were used for experiments.

Measurement of cytokines. Mice were intraperitoneally injected with 20 mg/kg LPS and bled 2 h after injection. Plasma concentrations of IL-1β, tumor necrosis factor alpha (TNF-α), IL-6, gamma interferon (IFN-γ), IL-12, and IL-18 were determined by enzyme-linked immunosorbent assay (ELISA) (Biosource). BMDM of mice with wild-type AhR (AhR WT mice) and AhR KO at 2×10^6 cells/ml were incubated with 10 ng/ml LPS for 8 h, and their culture supernatants were assessed for cytokines using mouse TNF-α and IL-1β ELISAs (Biosource).

Cell culture. All cells were maintained in RPMI medium (Sigma) supplemented with 10% fetal bovine serum (HyClone) and penicillin/streptomycin (Gibco) under 5.0% CO_2 at 37°C.

Caspase inhibitors. BMDM of AhR KO mice at 2×10^6 cells/ml were incubated with dimethyl sulfoxide (DMSO) or 80 μM Z-YVAD-FMK (caspase-1 inhibitor VI; Merck) or 100 μM Z-VAD-FMK (caspase inhibitor VI; Merck) for 30 min before LPS (10 ng/ml) stimulation. The BMDM were incubated for 8 h, and their culture supernatants were assessed for cytokines using a mouse IL-1β ELISA (Biosource).

Virus infections. Adenoviruses expressing green fluorescent protein (GFP), human Pai-2 (hPai-2), and human Bcl-2 (hBcl-2) were purchased from Vector Biolabs (Philadelphia). BMDM from AhR KO mice were infected for 12 h with adenoviruses expressing GFP, hPai-2, and hBcl-2 at a multiplicity of infection of 100. Infected BMDM were washed with PBS, followed by 12 h of incubation. As it was reported that adenoviral vectors enhanced IL-1β secretion in macrophages (19), IL-1β levels were investigated in these incubation supernatants by ELISA. At this point, no IL-1β was observed in the supernatants. Therefore, the cells were washed, collected with a scraper, and plated at 2×10^6 cells/ml in 96-well plates. The cells were treated with 10 ng/ml of LPS for an additional 8 h.

Retroviral infection was performed as follofws: pQC-mAhR, a cloned murine AhR (mAhR) fragment in pQCXIN (Clontech), and pQCXLN for LacZ expression (as a control) were transfected into PT67 cells that were then cultured for 24 h. The culture medium was replaced with fresh medium, and the culture was continued for an additional 24 h. This culture medium was used as the retrovirus particle source.

Microarray analysis. Total RNA samples were purified using Isogen before being processed and hybridized to Affymetrix mouse genome 430 2.0 arrays (Affymetrix). The experimental procedures for the GeneChip analyses were performed according to the Affymetrix technical manual.

Generation of stable transformant cell lines. ANA-1 cells were the kind gift of L. Varesio (3). ANA-1 cells were transduced with LacZ- or AhR-expressing retroviruses in a suspension with 8 mg/ml of Polybrene. One day after infection, the infected cells were replated and incubated in a selection medium containing 0.5 mg/ml of Geneticin (Gibco).

Plasmids. pcDNA3-p65 and pcDNA3-AhR were generated by inserting AhR and p65 cDNA fragments, excised from pBS-mAhR and pBS-mp65 (murine p65), into the pcDNA3 vector. The 2.7-kb fragment upstream of the Pai-2 transcription start site was generated by PCR (primers 5′-gaagcttGGGTTGCA GATCCCTTTAGC-3′ and 5′-ccatggtggCTGACACACAGGAAATGCTTC-3′; lowercase indicates restriction site sequences for cloning), using a BAC vector carrying the Pai-2 gene as a template, and then cloned into the pBS vector. After sequencing, the construct was cleaved with HindIII/NcoI, and the isolated insert was cloned into the HindIII/NcoI-digested pGL4.10 (Promega) to produce pGL4-Pai-2 (−2.7 kb). The 0.8-kb fragment upstream of the Pai-2 transcription start site was generated by PCR (primers 5′-ggaattcGAGAAGTGATCTGGTA GATG-3′ and 5′-ccatggtggCTGACACACAGGAAATGCTTC-3′) using pGL4-Pai-2 (−2.7 kb) as a template and cloned into the pBS vector. After sequencing, the construct was cleaved with HindIII/NcoI, and the isolated insert was cloned into the HindIII/NcoI-digested pGL4.10 (Promega) to produce pGL4-Pai-2 (−0.8 kb). pGL4-Pai-2 (−0.55 kb) was produced by cleaving pGL4-Pai-2 (−2.7 kb) with NdeI/EcoRV. pGL4-Pai-2 (−0.1 kb) was generated in a similar manner, using primers 5′-GATGTCTTTATGAGTAAAATGTTGAATCA-3′ and 5′-cca tggtggCTGACACACAGGAAATGCTTC-3′. pGL4-Pai-2 (−0.55 kb C/EBPβ mutant) was generated by site-directed mutagenesis using a Sculptor in vitro mutagenesis system (Amersham) with pGL4-Pai-2 (−0.55 kb) as a template and primer pair 5′-GATTTAAAATTGGAAAggGCTAAATTCTTGAATTTTGAA TGACATCAC-3′ and 5′-GTGATGTCATTCAAAATTCAAGAATTTAGCcc TTTCCAATTTTAAATC-3′.

RNA preparation and reverse transcription PCR (RT-PCR). Total RNA was prepared using Isogen (Nippon Gene, Tokyo) according to the manufacturer's protocol. cDNA synthesis from 1 μg of total RNA was carried out using Super-Script II reverse transcriptase (Invitrogen, United States). Real-time PCR was performed using an ABI7300 real-time PCR system (Applied Biosystems) and Platinum SYBR green quantitative PCR SuperMix (Invitrogen, United States). Each sample was normalized to the expression of β-actin as a control. The primer sequences were as follows: Pai-2, 5′-GCATCCACTGGCTTGGAA-3′ and 5′-GGGAATGTAGACCACAACATCAT-3′; Bcl-2, 5′-GTGGTGGAGGA ACTCTTCAGGGATG-3′ and 5′-GGTCTTCAGAGACAGCCAGGAGAAAT C-3′; AhR, 5′-TTCTATGCTTCCTCCACTATCCA-3′ and 5′-GGCTTCGTCC ACTCCTTGT-3′; Arnt, 5′-GGACGGTGCCATCTCGAC-3′ and 5′-CATCTG GTCATCATCGCATC-3′: Mmp-8, 5′-CCACACACAGCTTGCCAATGCC T-3′ and 5′-GGTCAGGTTAGTGTGTGTCCACT-3′; Nqo1, 5′-TTTAGGGTC GTCTTGGCAAC-3′ and 5′-AGTACAATCAGGGCTCTTCTCG-3′; AhR repressor, 5′-CCTGTCCCGGGATCAAAGATG-3′ and 5′-CTCACCACCAG AGCGAAGCCATTGA-3′; IL-1β, 5′-CTGAAGCAGCTATGGCAACT-3′ and 5′-GGATGCTCTCATCTGGACAG-3′; TNF-α, 5′-CTGTAGCCCACGTCGT AGC-3′ and 5′-TTGAGATCCATGCCGTTG-3′; Cox-2, 5′-GCATTCTTTGCC CAGCACTT-3′ and 5′-AGACCAGGCACCAGACCAAAG-3′; β-actin, 5′-GA CAGGATGCAGAAGGAGAT-3′ and 5′-TTGCTGATCCACATCTGCTG-3′; hPai-2, 5′-CCCAGAACCTCTTCCTCTCC-3′ and 5′-CATTGGCTCCCACTT CATTA-3′; and hBcl-2, 5′-GTGTGTGGAGAGCGTCAACC-3′ and 5′-GAGA CAGCCAGGAGAAATCAAA-3′.

Reporter assays. All luciferase assays were performed using a dual-luciferase reporter assay system according to the manufacturer's protocol (Promega), with some modifications. RAW 264.7 cells (2.0×10^4 cells/well) were plated in 24-well plates 24 h prior to transfection. Cells were cotransfected with 100 ng pGL4-Pai-2 (various lengths in kilobases) (see "Plasmids"), 1 ng *Renilla* luciferase (as an internal control), and 1 ng pcDNA3-p65 and/or pcDNA3-AhR using Fu-GENE HD transfection reagent (Roche) according to the manufacturer's protocol. All cells were incubated for 12 h at 37°C after transfection, treated with 10 ng/ml LPS, and incubated for an additional 6 h.

Co-IP assays. AhR WT PEMs or transfected 293T cells were washed with ice-cold PBS, followed by buffer containing 20 mM HEPES, pH 7.4, 125 mM NaCl, 1% Triton X-100, 10 mM EDTA, 2 mM EGTA, 2 mM Na_3VO_4, 50 mM sodium fluoride, 20 mM $ZnCl_2$, 10 mM sodium pyrophosphate (31). The cells were harvested by scraping, centrifuged at 5,000 rpm at 4°C for 5 min, and suspended in immunoprecipitation (IP) buffer containing a protease inhibitor cocktail (Roche). The cells were vortexed and placed on ice for 10 min. The samples were then centrifuged at 15,000 rpm for 5 min at 4°C, and the supernatants were saved as whole-cell lysates.

The prepared whole-cell lysate (250 μl) was incubated with anti-immunoglobulin G, anti-AhR antibody, or anti-p65 for 2 h at 4°C. The reaction mixture was supplemented with 20 μl of protein A-agarose beads (Amersham). After being incubated for an additional 1 h at 4°C, the beads were washed three times with IP buffer containing protease inhibitor cocktail and resuspended in sodium dodecyl sulfate (SDS) sample buffer. The coimmunoprecipitated proteins were resolved by SDS-polyacrylamide gel electrophoresis (PAGE), and Western blot analysis was performed.

ChIP assays. Chromatin IP (ChIP) assays were performed with PEMs from AhR WT and AhR KO mice. PEMs were stimulated with 10 ng/ml LPS for 60 min and then fixed with formaldehyde for 10 min. The cells were lysed and sheared by sonication. The lysis solution was incubated with immunoglobulin G or preimmune serum and protein A-agarose for 2 h to remove nonspecific DNA binding. The solution was incubated overnight with a specific antibody, followed by incubation with protein A-agarose saturated with salmon sperm DNA. Precipitated DNA was analyzed by real-time PCR using primer pair 5′-GGAAGT TCCCTGAGGCTTATAGG-3′ and 5′-ATGGAAGCACATACATAAGAACA